



OPEN ACCESS

EDITED BY

Liang Zhang,
China University of Geosciences, China

REVIEWED BY

Xiaowei Li,
China University of Geosciences, China
Xin shang Bao,
Chang'an University, China
Jinbao Yang,
Guilin University of Technology, China

*CORRESPONDENCE

Dapeng Li,
dpengli@126.com
Zhigang Song,
zgsong@sdu.edu.cn

SPECIALTY SECTION

This article was submitted to
Geochemistry,
a section of the journal
Frontiers in Earth Science

RECEIVED 16 September 2022

ACCEPTED 01 November 2022

PUBLISHED 09 January 2023

CITATION

Wei P, Li D, Song Z, Liu Q, Geng K, Zhang Y, Ding C, Cai N, Li Z, Zhang C and Xie W (2023), Petrogenesis and relationship with REE mineralization of the quartz syenite from Chishan and Longbaoshan alkaline complex, southeastern North China Craton: Insights from zircon U–Pb geochronology, element, and Sr–Nd–Pb–Hf isotope geochemistry. *Front. Earth Sci.* 10:1046071. doi: 10.3389/feart.2022.1046071

COPYRIGHT

© 2023 Wei, Li, Song, Liu, Geng, Zhang, Ding, Cai, Li, Zhang and Xie. This is an open-access article distributed under the terms of the [Creative Commons Attribution License \(CC BY\)](https://creativecommons.org/licenses/by/4.0/). The use, distribution or reproduction in other forums is permitted, provided the original author(s) and the copyright owner(s) are credited and that the original publication in this journal is cited, in accordance with accepted academic practice. No use, distribution or reproduction is permitted which does not comply with these terms.

Petrogenesis and relationship with REE mineralization of the quartz syenite from Chishan and Longbaoshan alkaline complex, southeastern North China Craton: Insights from zircon U–Pb geochronology, element, and Sr–Nd–Pb–Hf isotope geochemistry

Pengfei Wei¹, Dapeng Li^{1*}, Zhigang Song^{1,2*}, Qiang Liu¹, Ke Geng¹, Yan Zhang¹, Chengwu Ding³, Na Cai¹, Zengsheng Li¹, Chao Zhang¹ and Wei Xie¹

¹Shandong Institute of Geological Sciences, Key Laboratory of Gold Mineralization Processes and Resources Utilization, Ministry of Natural Resources, Shandong Provincial Key Laboratory of Metallogenic Geological Processes and Resource Utilization in Metallic Minerals, Jinan, China, ²College of Earth Science and Engineering, Key Laboratory of Depositional Mineralization and Sedimentary Mineral of Shandong Province, Shandong University of Science and Technology, Qingdao, China, ³Shandong University of Technology, Zibo, China

Mesozoic alkaline complexes associated with the rare earth element (REE) mineralization are developed in southeastern North China Craton (NCC), and they recorded some important information about the lithospheric thinning and destruction of the NCC. Zircon U–Pb dating results reveal that syenitic rocks from the Chishan and Longbaoshan alkaline complexes were emplaced at ca. 126.2–123.7 Ma. These syenitic rocks have an arc-like affinity with enriched LREEs and LILEs (e.g., Ba and Th) and depleted HFSE (e.g., Nb and Ta). However, they plot within the extensional alkaline–calc–alkaline field in the Ig (CaO/(K₂O + Na₂O)) versus SiO₂ discrimination diagram and plot within the fields of the divergent plate and within-plate settings in the Nb_N versus Th_N discrimination diagram, implying an extensional tectonic setting. Thus, we suggest that the syenitic rocks should form in an extensional tectonic settings related to rollback and retreat of the subducting Paleo-Pacific plate. These syenitic rocks have similar Sr–Nd–Pb–Hf isotope compositions ($(^{87}\text{Sr}/^{86}\text{Sr})_i = 0.7062$ to 0.7101, $\epsilon_{\text{Nd}}(t) = -8.2$ to -15.0 , $\epsilon_{\text{Hf}}(t) = -13.5$ to -9.6), which are the same as the enriched subcontinental lithospheric mantle (SCLM) of the NCC. Taking into account not only our new data but also previously published data regarding the evolution of NCC in the Mesozoic, we conclude that the syenitic rocks from the Chishan and Longbaoshan complexes are derived from partial melting of the lithospheric mantle triggered by the Paleo-Pacific plate subduction. Moreover, the

geochemical and Sr–Nd–Pb isotopic similarity between the Chishan REE ores, Longbaoshan altered rocks, and the syenitic rocks implied that they are homologous products of Early Cretaceous and that the mineralization shows inheritance to the magmatic hydrothermal evolution.

KEYWORDS

zircon U–Pb dating, Sr–Nd–Pb isotope composition, alkaline complexes, enriched lithospheric mantle, REE mineralization

1 Introduction

The North China Craton (NCC) is the largest cratonic area at the easternmost point of Eurasia (Yang et al., 2020). It experienced extensive destruction and lithospheric thinning during the Mesozoic (Fan et al., 2000; Goss et al., 2010; Zhai and Santosh, 2011; Zhu et al., 2011; Li and Santosh, 2017; Yang et al., 2018a; Yang et al., 2018b; Yang and Santosh, 2020). This transformation and destruction disturbed the stability of the coupling between the crust and lithospheric mantle and caused activation of the crust, which led to eruption of large-scale magmatism and mineralization during the Mesozoic (Wu et al., 2005; Chen et al., 2007; Goldfarb and Santosh, 2014). Although controversies about the timing, tectonic setting, and mechanism of the lithospheric thinning remain hotly continued (Gao et al., 2002; Zhang H. F. et al., 2007; Wu et al., 2008; Santosh, 2010; Zhu et al., 2011; Zhang et al., 2013), it is generally accepted that the interaction between the crust and the mantle had an important impact during this process (Wilde, et al., 2003; Xu et al., 2004; Gao et al., 2008). Alkaline rocks, as a kind of mantle-derived intrusions, are generally developed in extensional settings (Tu et al., 1984; Qiu, 1993), for instance, post-collisional extension (Bonin et al., 1998) or along deep faults (Jung et al., 2007). They are considered one of the ideal options to study the crust–mantle interaction and continental crust evolution (Yang et al., 2007; Lan et al., 2011).

There are a large number of magmatic rocks related to NCC destruction during the Mesozoic, especially the widespread late Mesozoic alkaline rocks in the Luxi Block, southeastern NCC (Zhang et al., 2005; Lan et al., 2011). These magmatic rocks recorded some important information about lithospheric thinning and destruction of the NCC (Xu et al., 2004; Zhang et al., 2005; Lan et al., 2011; Yang D. B. et al., 2012; Zhang et al., 2014; Yang et al., 2018a), including the lithospheric architecture, crust–mantle interaction, tectonic reactivation, timing, mechanism, and geodynamic setting (Gao et al., 2002; Wu et al., 2008; Santosh, 2010; Zhu et al., 2011; Deng et al., 2018; Yang et al., 2020). Moreover, alkaline rocks in the Luxi Block have a close relationship with the gold and rare earth element (REE) mineralization. For instance, the Longbaoshan complex, which is relatively larger than other alkaline intrusions in the Luxi Block, is closely associated with the mineralization of gold and REE deposits. The Chishan alkaline complex is considered the ore-forming parent rock of the Chishan REE deposit, which

holds the third-largest light REE deposit in China, after the Inner Mongolia Bayan Obo and Sichuan Maoniuping REE deposits. With regard to the Longbaoshan and Chishan complexes, the lithologic assemblage is dominated by syenitic rocks, which are the most closely related to REE mineralization. However, the petrogenesis of these syenitic rocks has not been systematically researched until now (Zhang et al., 2005; Lan et al., 2011). In this study, we carried out detailed fieldwork, petrological and mineralogical observations, and obtained element geochemical, zircon U–Pb–Hf isotopic, and Sr–Nd–Pb isotopic data of the quartz syenite from the Longbaoshan and Chishan complexes to identify the nature and petrogenesis of the syenitic rocks and to understand their significance to the crust–mantle interaction. The final goal, using the results from the Longbaoshan and Chishan complexes, is to further our understanding on how magmatic processes control REE enrichment in alkaline magmas in southeastern NCC.

2 Geological background and sampling

2.1 Geological background

The NCC is China's oldest and largest craton due to its 2.5–3.8 Ga Archean core (Liu et al., 1992). It is separated from the Yangtze Craton by the Qinling–Dabie–Sulu Orogenic Belt to the south and east and from the Central Asian Orogenic Belt by the Bayan Obo–Chifeng–Kaiyuan fault to the north (Figure 1A) (Li et al., 1993; Zhao et al., 2001). In many popular models, the NCC is divided into the Western Block (WB) and Eastern Block (EB), which were welded along the nearly north–south trending Trans-North China Orogen (TNCO) (Zhao et al., 2001; Zhao and Zhai, 2013). The basement rocks within the EB are primarily dominated by Archean to Paleoproterozoic tonalite–trondhjemite–granodiorite (TTG) (Zhao and Zhai, 2013). The WB was the outcome of amalgamation between the Ordos and Yinshan blocks along the Khondalite Belt at 1.95–1.92 Ga (Santosh, 2010; Yang et al., 2018a). The TNCO is a collision orogenic belt between the EB and WB in the Paleoproterozoic (1.85 Ga), with basement rocks of late Neoproterozoic–Paleoproterozoic TTG gneisses and granitoids (Zhao et al., 2005).

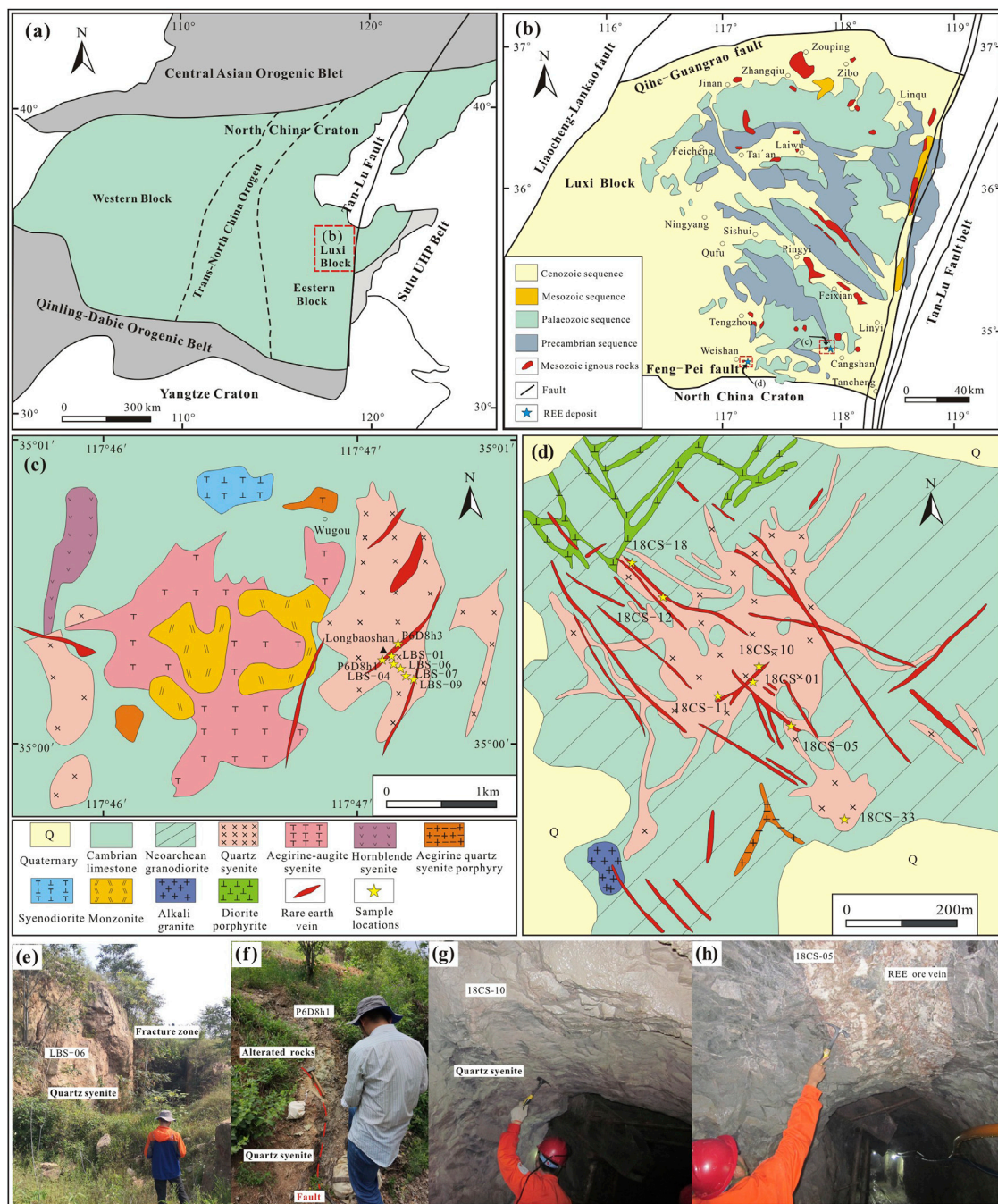


FIGURE 1 (A) Simplified geological map of the North China Craton and the location of the Luxi Block (after Zhao et al., 2001; Zhang et al., 2005). (B) Simplified geological map of the Luxi Block (after Zhang H. F. et al., 2007). (C) Simplified geological map of the Longbaoshan alkaline complex (after Lan et al., 2011). (D) Simplified geological map of the Chishan alkaline complex (Wei et al., 2019). (E–H) Photos of field outcrops where the four kinds of samples were collected in.

The Luxi Block is bordered by the Tan-Lu fault in the east, the Liaocheng–Lankao fault in the west, the Qihé–Guangrao fault in the north, and the Fengpei fault in the south (Figure 1B) (Zhang X. M. et al., 2007). The crystalline basement of the Luxi

Block incorporates a suite of Neoproterozoic metamorphic rocks (e.g., gneiss, amphibolite, and deformed/metamorphosed TTG) and Paleoproterozoic granitoids. The sedimentary cover is mainly composed of Paleozoic carbonates and clastic rocks,

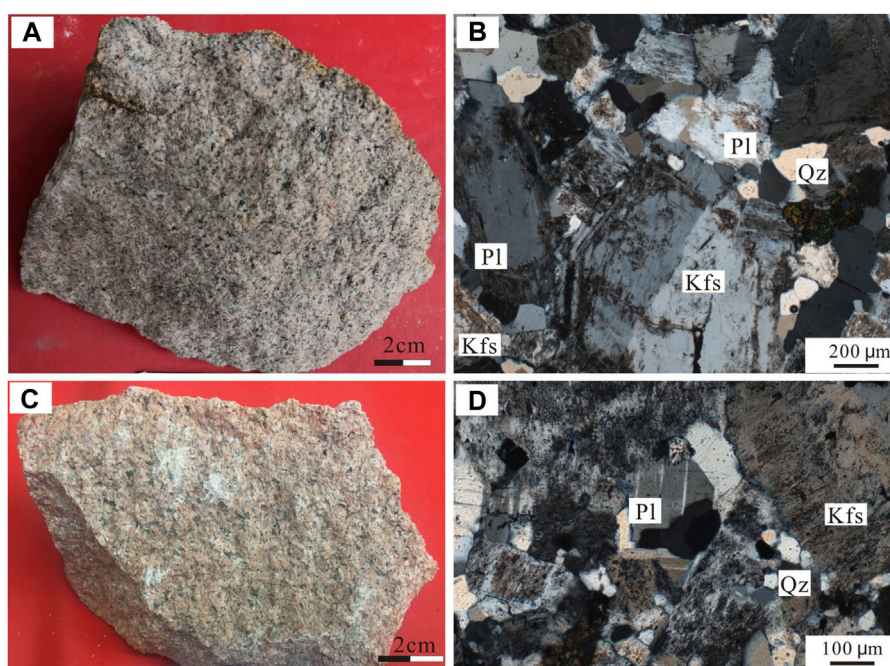


FIGURE 2

Photographs of the quartz syenite (A,B) from the Chishan complex and porphyritic quartz syenite (C,D) from the Longbaoshan complex. Abbreviations: Kfs = K-feldspar, Pl = plagioclase, and Qtz = quartz.

Mesozoic to Cenozoic terrigenous clastic rocks, and volcanoclastic rocks. In addition, some intermediate-basic rocks, mafic dikes, and alkaline rocks are also exposed (Figure 1B) (Xu et al., 2015; Wang et al., 2018; Yang et al., 2020). Especially in the Jurassic–Early Cretaceous period, a large number of alkaline rocks were developed as batholiths, stocks, or dykes (Wei et al., 2019). Their lithology was mainly syenite, syenite porphyrite, diorite porphyrite, diabase, and lamprophyre. The representative alkaline rocks are the Tongshi complex, Shagou complex, Chishan alkaline complex, and Longbaoshan alkaline complex. The Longbaoshan alkaline complex, with an area of 3.5 km², is exposed near the Wugou village of the Cangshan county. It is predominantly composed of quartz syenite, syenite, aegirine–augite syenite, and syenodiorite assemblages (Figure 1C). The NW-trending Longhui fault is the major structure in the study area, and its SN-, EW-, and NNE-trending secondary fracture and alteration zone are developed, controlling the distribution of the Longbaoshan complex and REE ore veins (Figures 1E,F). The Chishan alkaline complex covers an area of 0.5 km² and crops out in the Chishan village of the Weishan county. It mainly consists of quartz syenite, alkali granite, and aegirine quartz syenite (Figure 1D). The regional structure mainly comprises the NW-, NE-, SN-, and EW-trending faults. The Chishan complex extends in NE- and SW-trending controlled by the regional faults and contacts with gneiss in irregular branches. The

REE ore veins occurred within the quartz and gneiss (Figures 1D,H).

2.2 Samples

In this study, five samples of quartz syenite (18CS-01, -10, -11, -12, and -33) and two samples of REE ore (18CS-05 and 18CS-18) were collected from the -160 m level of the Chishan REE deposit (Figures 1D,G,H). A total of five samples of porphyritic quartz syenite samples (LBS-01, -04, -06, -07, and -09) and two samples of altered rock (P6D8h1 and P6D8h3) were collected from outcrops (Figures 1C,E,F) of the Longbaoshan alkaline complex. Petrographic observations, whole-rock geochemical, and Sr–Nd–Pb isotopic analyses were performed on all the samples. The zircon U–Pb dating and Hf isotopic analyses were conducted only on samples 18CS-01 and LBS-01.

The quartz syenite of the Chishan alkaline complex, with gray to light pink color, has generally porphyroid or porphyritic textures and a massive structure (Figure 2A). It consists mainly of K-feldspar (53 vol%), plagioclase (25 vol%), quartz (15 vol%), and hornblende (5 vol%). The K-feldspar grains have grain sizes of 1.0–1.5 mm and are subhedral columnar or granular, some of which show Carlsbad twinning (Figure 2B). The porphyritic quartz syenite of the Longbaoshan complex is generally gray

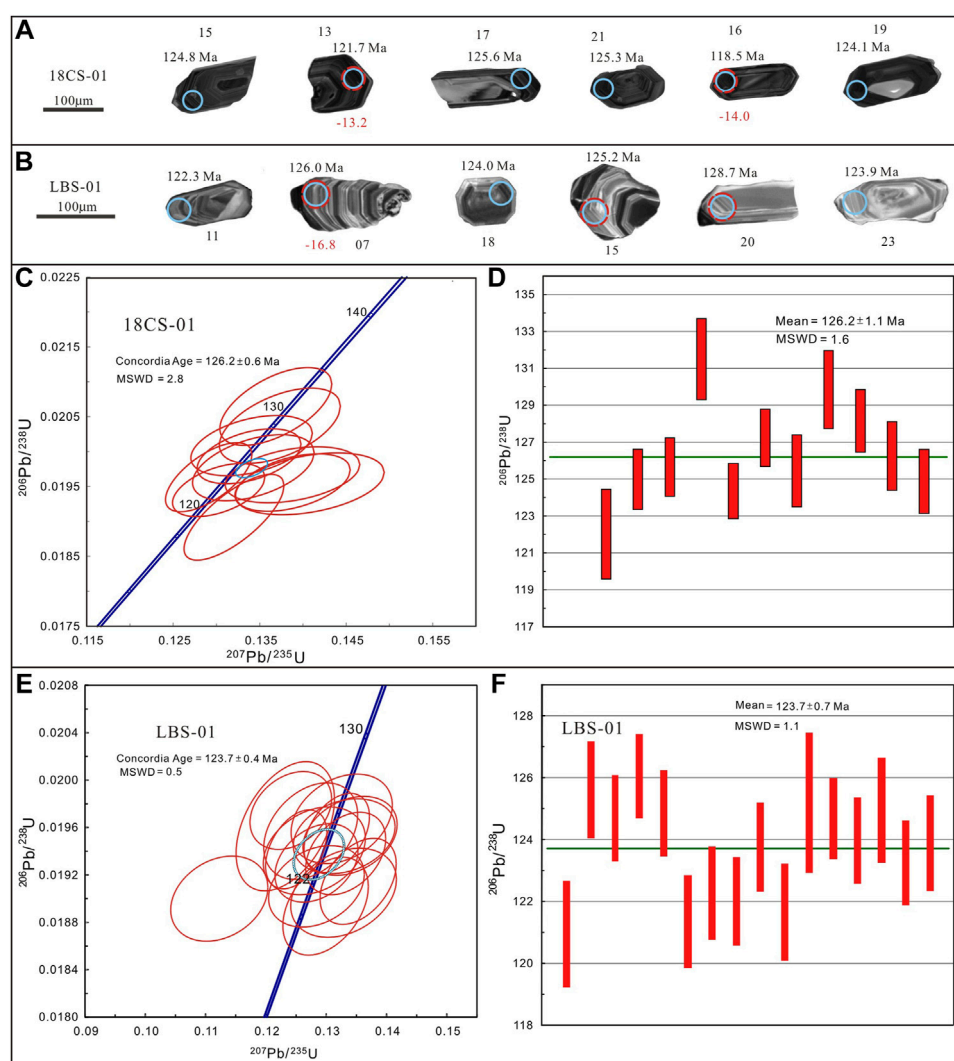


FIGURE 3

(A, B) Cathodoluminescence (CL) images of representative zircon grains in sample 18CS-01 and LBS-01, showing analytical positions, $^{206}\text{Pb}/^{238}\text{U}$ ages, and $\epsilon_{\text{Hf}}(t)$ values. (C–F) U–Pb concordia diagram and weighted mean $^{206}\text{Pb}/^{238}\text{U}$ ages of zircons from Chishan and Longbaoshan complexes.

to light pink in color and shows a porphyritic texture (Figure 2C). K-feldspar (1.0–2.5 mm), plagioclase (0.3–1.0 mm), and quartz (0.1–0.3 mm) phenocrysts are distributed in the groundmass (Figure 2D), while the matrix is dominated by K-feldspar, plagioclase, and quartz with sizes of 0.01–0.05 mm.

3 Analytical methods

3.1 Zircon LA-ICP-MS U–Pb dating

Zircon separation was conducted using standard density and magnetic separation techniques followed by hand-picking at Langfang Fengzeyuan Rock and Mineral Testing Technology

Co., Ltd. (Langfang, China). The zircons grains were selected under a stereo-microscope, sealed in an epoxy resin target, and polished until the mid-sections were exposed. Cathodoluminescence (CL) transmitted and reflected images were taken prior to U–Pb dating analysis to identify the internal textures of zircon grains and select target spots with no cracks, no inclusions, and good growth zones for U–Pb dating and Hf isotopic analysis.

Zircon U–Pb dating was conducted at Beijing Createch Testing Technology Co., Ltd. (Beijing, China) using a Neptune multi-collector inductively coupled plasma mass spectrometry (MC-ICP-MS) equipped with a New Wave 193-nm laser sampler. The diameter of the laser beam was 35 μm , and the carrier gas was He. Detailed analytical processes were

TABLE 1 LA-ICP-MS zircon U–Pb isotope analyses of the quartz syenite from Chishan and Longbaoshan complexes.

Spots	Content (ppm)			$^{232}\text{Th}/^{238}\text{U}$	Ratio/deviation						Age (Ma)/deviation						Concordance
	Th ²³²	U ²³⁸	Pb		$^{207}\text{Pb}/^{206}\text{Pb}$	1 σ	$^{207}\text{Pb}/^{235}\text{U}$	1 σ	$^{206}\text{Pb}/^{238}\text{U}$	1 σ	$^{207}\text{Pb}/^{206}\text{Pb}$	1 σ	$^{207}\text{Pb}/^{235}\text{U}$	1 σ	$^{206}\text{Pb}/^{238}\text{U}$	1 σ	
18CS-01 Quartz syenite ^a																	
18CS-01-13	788.5	1671.6	103.37	0.47	0.0505	0.0010	0.1320	0.0025	0.0191	0.0003	216.7	44.4	125.9	2.3	121.7	1.7	96%
18CS-01-15	586.9	1444.8	83.75	0.41	0.0516	0.0012	0.1388	0.0029	0.0196	0.0002	333.4	53.7	132.0	2.6	124.9	1.1	94%
18CS-01-16	1576.0	1557.1	167.32	1.01	0.0526	0.0011	0.1345	0.0030	0.0186	0.0002	322.3	52.8	128.2	2.7	118.5	1.3	92%
18CS-01-17	332.9	1256.5	57.45	0.26	0.0511	0.0012	0.1388	0.0034	0.0197	0.0002	255.6	53.7	132.0	3.1	125.6	1.1	95%
18CS-01-18	228.6	1247.1	48.29	0.18	0.0480	0.0009	0.1369	0.0028	0.0206	0.0002	101.9	42.6	130.2	2.5	131.7	1.5	98%
18CS-01-19	823.8	1948.8	108.82	0.42	0.0485	0.0008	0.1303	0.0023	0.0194	0.0002	124.2	37.0	124.3	2.1	124.2	1.1	99%
18CS-01-20	660.9	1571.5	90.21	0.42	0.0486	0.0009	0.1338	0.0026	0.0199	0.0002	131.6	42.6	127.5	2.4	127.2	1.1	99%
18CS-01-21	420.8	1472.0	65.17	0.29	0.0477	0.0007	0.1291	0.0022	0.0196	0.0002	83.4	32.4	123.3	2.0	125.3	1.4	98%
18CS-01-22	156.6	737.6	28.85	0.21	0.0490	0.0011	0.1373	0.0031	0.0204	0.0002	150.1	58.3	130.7	2.7	130.0	1.5	99%
18CS-01-23	278.2	755.6	39.66	0.37	0.0484	0.0011	0.1341	0.0031	0.0201	0.0002	120.5	47.2	127.7	2.8	128.2	1.2	99%
18CS-01-24	431.8	1025.0	53.69	0.42	0.0492	0.0010	0.1343	0.0031	0.0198	0.0002	166.8	48.1	127.9	2.8	126.2	1.3	98%
18CS-01-25	542.3	1066.9	70.03	0.51	0.0520	0.0012	0.1408	0.0038	0.0195	0.0002	287.1	54.6	133.7	3.4	124.7	1.2	93%
LBS-01 Porphyritic quartz syenite																	
LBS-01-01	358.3	274.8	39.69	1.30	0.0501	0.0019	0.1299	0.0047	0.0189	0.0003	211.2	95.4	124.0	4.2	120.9	1.7	97%
LBS-01-03	368.3	263.3	41.42	1.40	0.0491	0.0021	0.1326	0.0055	0.0197	0.0002	153.8	102.8	126.4	5.0	125.6	1.6	99%
LBS-01-05	432.9	275.1	46.46	1.57	0.0496	0.0017	0.1339	0.0052	0.0195	0.0002	172.3	76.8	127.6	4.6	124.7	1.4	97%
LBS-01-07	456.0	338.4	49.93	1.35	0.0458	0.0017	0.1241	0.0045	0.0197	0.0002	100.1	77.8	118.8	4.0	126.0	1.4	94%
LBS-01-09	640.9	441.4	69.31	1.45	0.0490	0.0014	0.1317	0.0036	0.0196	0.0002	150.1	66.7	125.7	3.2	124.8	1.4	99%
LBS-01-11	449.6	387.9	50.98	1.16	0.0515	0.0017	0.1353	0.0042	0.0191	0.0002	264.9	76.8	128.8	3.7	122.3	1.5	94%
LBS-01-12	227.9	211.1	28.56	1.08	0.0490	0.0021	0.1284	0.0052	0.0191	0.0002	150.1	93.5	122.6	4.7	122.0	1.4	99%
LBS-01-13	590.1	375.5	64.84	1.57	0.0498	0.0015	0.1332	0.0044	0.0194	0.0002	183.4	65.7	127.0	3.9	123.7	1.5	97%
LBS-01-14	224.1	193.9	24.67	1.16	0.0507	0.0022	0.1329	0.0058	0.0190	0.0002	227.8	98.1	126.7	5.2	121.6	1.6	95%
LBS-01-15	294.3	282.8	37.27	1.04	0.0460	0.0023	0.1232	0.0054	0.0196	0.0004	183.4	65.7	118.0	4.9	125.2	2.3	94%
LBS-01-17	250.7	239.2	30.02	1.05	0.0496	0.0020	0.1330	0.0056	0.0195	0.0002	176.0	128.7	126.8	5.0	124.7	1.3	98%
LBS-01-18	620.8	600.8	71.74	1.03	0.0468	0.0013	0.1250	0.0034	0.0194	0.0002	39.0	66.7	119.6	3.0	124.0	1.4	96%
LBS-01-19	338.8	241.8	37.38	1.40	0.0481	0.0022	0.1274	0.0051	0.0196	0.0003	101.9	103.7	121.8	4.6	124.9	1.7	97%
LBS-01-22	379.0	350.5	41.58	1.08	0.0485	0.0018	0.1284	0.0045	0.0193	0.0002	120.5	87.0	122.6	4.1	123.2	1.4	99%
LBS-01-23	295.5	206.9	31.16	1.43	0.0482	0.0021	0.1280	0.0056	0.0194	0.0002	105.6	-97.2	122.3	5.0	123.9	1.5	98%

^aNote: The quartz syenite zircon U–Pb data are obtained from previously published work (Wei et al., 2019).

described by Yuan et al. (2004). The results were corrected with the measured ^{204}Pb for U–Th–Pb isotopic fractionation and the presence of common Pb (from the measured ^{204}Pb). The final data were processed with ICP-MS DataCal software (Liu et al., 2008). Zircon U–Pb concordia diagrams and mean ages were obtained with ISOPLOT 3.0 software (Ludwig, 2003).

3.2 Major and trace elements

The major and trace element concentrations were determined at Beijing Createch Testing Technology Co., Ltd. (Beijing, China). Fresh samples were crushed to less than 200 meshes. Major elements were analyzed by X-ray fluorescence spectrometry (XRF-1800), with an accuracy of better than 1%. Fused glass disks were prepared by mixing the samples with $\text{Li}_2\text{B}_4\text{O}_7$ – LiBO_2 flux, with an automated fusion system. The trace elements were analyzed using the lithium borate melting method and determined by quantitative ICP-MS (Agilent 7500ce), with an accuracy of better than 5%.

3.3 Whole rock Sr–Nd–Pb isotopes

Whole rock Sr, Nd, and Pb isotopes were determined in Beijing Createch Testing Technology Co., Ltd. (Beijing, China) by using a Finnigan MAT 262 multi-channel thermal ionization mass spectrometer (TIMS). Samples were weighted into Teflon capsules along with ^{84}Sr , ^{87}Rb , ^{150}Nd , and ^{147}Sm isotopic spikes and then digested in HClO_4 and HF. The separation of lead was used as the conventional anionic resin-exchange technique with HCl. After ion exchange separation, the Sr–Nd isotope ratios were analyzed using a Finnigan MAT 262 thermal ionization mass spectrometer. The chemical analytical procedures were described by Pin et al. (2014).

The correction of Sr and Nd isotope ratios mass fractionation used were $^{87}\text{Sr}/^{88}\text{Sr} = 0.1194$ and $^{146}\text{Nd}/^{144}\text{Nd} = 0.7219$, respectively. The procedural blanks for Rb and Sr were <100 pg, and for Sm and Nd were <50 pg. The obtained standard results are as follows: NBS-987 $^{87}\text{Sr}/^{86}\text{Sr} = 0.710248 \pm 13$; GSB $^{143}\text{Nd}/^{144}\text{Nd} = 0.512185 \pm 8$. Repeated analyses of BCR-2 standard yielded the ratio of $^{206}\text{Pb}/^{204}\text{Pb} = 18.7477 \pm 3$, $^{207}\text{Pb}/^{204}\text{Pb} = 15.6111 \pm 3$, and $^{208}\text{Pb}/^{204}\text{Pb} = 38.6921 \pm 7$, respectively, and all of them are within the error range (Yang et al., 2010).

3.4 Zircon Lu–Hf isotopes

The zircon Lu–Hf isotope analysis was proceeded on or close to the U–Pb dating spots at Beijing Createch Testing Technology Co., Ltd. (Beijing, China) using a Neptune MC-ICP MS system. The laser and mass spectrometry conditions are the same with the zircon U–Pb dating. Analytical conditions, instrument

settings, and procedures were described by Geng et al. (2011). In this study, the adopted ^{176}Lu decay constant was $1.867 \times 10^{-11} \text{year}^{-1}$ (Söderlund et al., 2004), the $^{176}\text{Hf}/^{177}\text{Hf}$ ratio value of chondrite was 0.0332, and the $^{176}\text{Lu}/^{177}\text{Hf}$ ratio value was 0.282772 (Blichert-Toft and Albarède, 1997). Depleted mantle model ages (t_{DM1}) were calculated based on present-day depleted mantle $^{176}\text{Lu}/^{177}\text{Hf}$ and $^{176}\text{Hf}/^{177}\text{Hf}$ ratios ($^{176}\text{Lu}/^{177}\text{Hf} = 0.0384$, $^{176}\text{Hf}/^{177}\text{Hf} = 0.28325$) (Griffin et al., 2000). The $^{176}\text{Lu}/^{177}\text{Hf}$ ratio of 0.015 (Griffin et al., 2002) was used to calculate the depleted mantle model age (t_{DM2}). The detailed analysis and calculation procedures were described by Wu et al. (2007).

4 Results

4.1 Zircon U–Pb dating

Zircon grains from sample 18CS-01 (quartz syenite) of the Chishan complex are dark in color and euhedral to short columnar in shape, with the sizes of 100–200 μm and aspect ratios from 1:2.5 to 1:1.25. The CL images show that most of the grains have smooth surfaces and oscillatory zoning, indicative of a magmatic origin (Figure 3A). Zircon grains from sample LBS-01 (porphyritic quartz syenite) of the Longbaoshan complex are light black to colorless. They are euhedral to subhedral and range in size from 50 to 150 μm , with aspect ratios of 1:1 to 1:2.5. In the CL images, most zircon grains also display obvious oscillatory zonation (Figure 3B).

A total of 50 spots from two samples were analyzed in this study. In order to ensure the accuracy and reliability of the results, age data having the concordance below 90% in the $^{207}\text{Pb}/^{235}\text{U}$ – $^{206}\text{Pb}/^{238}\text{U}$ plot were deleted. The adjusted data are listed in Table 1.

Zircons from Chishan quartz syenite have ^{238}U contents of 738–1672 ppm, ^{232}Th concentrations of 157–1576 ppm, and $^{232}\text{Th}/^{238}\text{U}$ ratios of 0.18–1.01. The $^{206}\text{Pb}/^{238}\text{U}$ ages of all the analyzed zircons are concentrated and fall on the concordia line (Figure 3C) and yield a mean age of 126.2 ± 1.1 Ma (MSWD = 1.6) (Figure 3D), which is considered to be the crystallization age of the quartz syenite.

Zircons from Longbaoshan porphyritic quartz syenite have ^{238}U contents of 194–601 ppm, ^{232}Th concentrations of 224–641 ppm, and $^{232}\text{Th}/^{238}\text{U}$ ratios of 1.08–1.57. The $^{206}\text{Pb}/^{238}\text{U}$ ages of all the analyzed zircons fall on or near the concordia line (Figure 3E) and yield a mean age of 123.7 ± 0.7 Ma (MSWD = 1.1) (Figure 3F). It is suggested that the porphyritic quartz syenite was emplaced contemporaneous with the quartz syenite (18CS-01) in the Early Cretaceous.

4.2 Major and trace elements

Major and trace element contents and associated parameters of all samples from the Longbaoshan and Chishan complexes are

TABLE 2 Whole-rock major and trace element compositions of the quartz syenite, REE ore samples, and altered rocks from Chishan and Longbaoshan REE deposits.

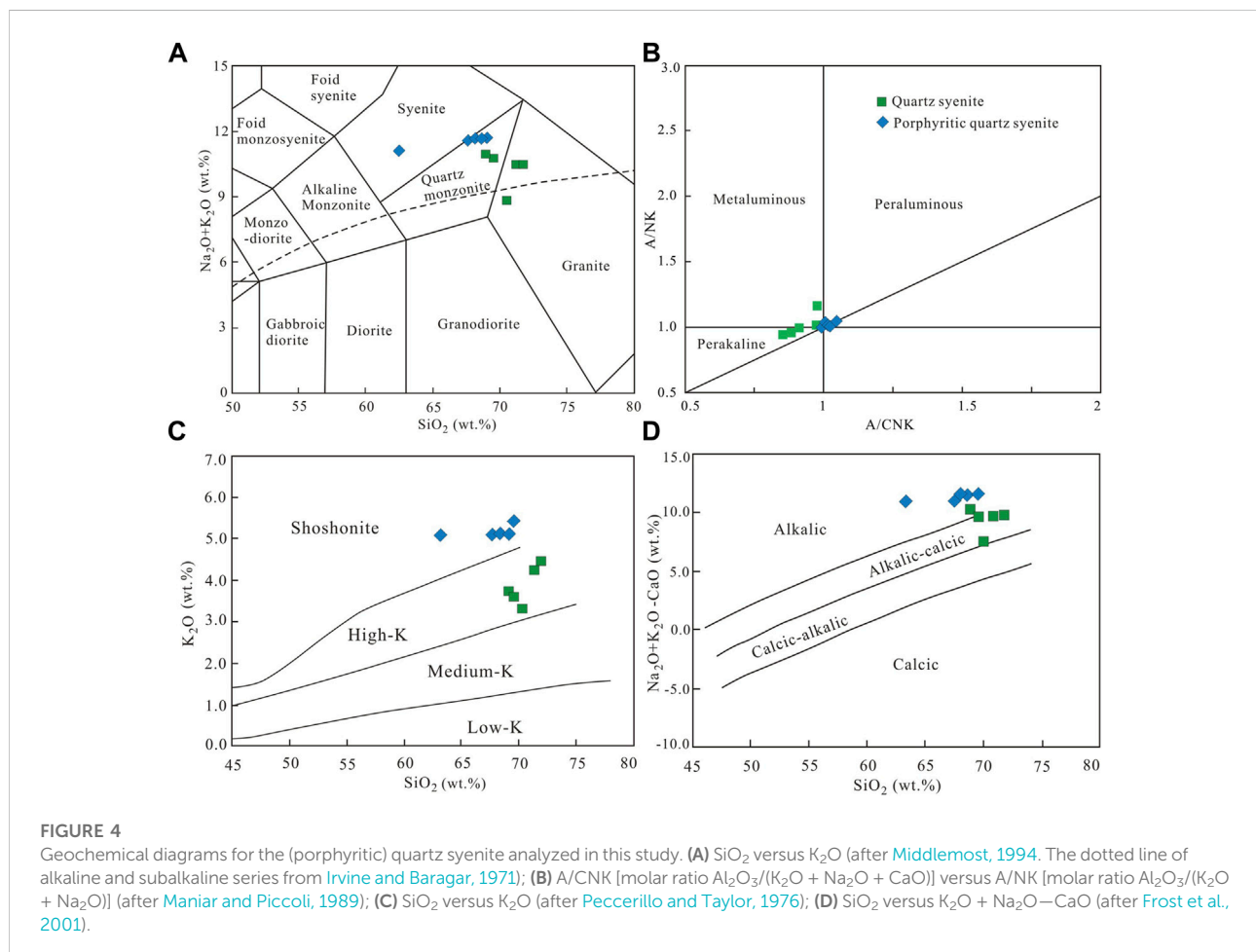
Sample number	18CS-01	18CS-10	18CS-11	18CS-12	18CS-33	18CS-05	18CS-18	LBS-01	LBS-04	LBS-06	LBS-07	LBS-09	P6D8h1	P6D8h3
Rock type	Quartz syenite ^a					REE ore		Porphyritic quartz syenite					Altered rocks	
SiO ₂	70.20	71.35	71.72	69.02	69.42	—	—	67.53	68.82	69.01	68.42	62.87	—	—
Al ₂ O ₃	15.25	13.74	13.51	16.12	15.41	—	—	17.03	16.77	16.85	16.96	17.64	—	—
MgO	0.49	0.16	0.19	0.15	0.48	—	—	0.27	0.07	0.07	0.08	0.74	—	—
Na ₂ O	5.53	6.25	6.12	7.13	7.11	—	—	6.80	6.84	6.75	6.89	6.61	—	—
K ₂ O	3.34	4.29	4.43	3.82	3.67	—	—	5.02	5.08	5.21	5.06	5.08	—	—
P ₂ O ₅	0.07	0.03	0.04	0.10	0.11	—	—	0.06	0.04	0.04	0.04	0.27	—	—
TiO ₂	0.17	0.08	0.06	0.11	0.11	—	—	0.19	0.16	0.16	0.16	0.24	—	—
CaO	1.59	0.73	0.74	0.38	1.15	—	—	0.41	0.19	0.19	0.16	1.49	—	—
TFe ₂ O ₃	1.32	2.35	2.31	1.38	1.50	—	—	2.04	1.41	1.36	1.48	3.02	—	—
MnO	0.02	0.13	0.12	0.05	0.05	—	—	0.03	0.01	0.01	0.01	0.06	—	—
LOI	2.45	0.77	0.71	0.96	0.63	—	—	0.56	1.18	0.92	1.37	0.98	—	—
TOTAL	100.4	99.9	99.9	99.2	99.7	—	—	99.9	100.6	100.6	100.6	99.0	—	—
Na ₂ O+K ₂ O	8.87	10.53	10.56	10.94	10.78	—	—	11.82	11.91	11.95	11.95	11.69	—	—
A/NK	1.199	0.921	0.908	1.017	0.983	—	—	1.02	1.00	1.01	1.01	1.08	—	—
A/CNK	0.977	0.846	0.833	0.974	0.867	—	—	0.98	0.98	0.99	0.99	0.92	—	—
Rb	55	103	110	53	54	34	31	129	108	111	107	108	146	225
Sr	1236	340	338	831	1381	61432	73381	598	372	416	297	2742	491	1407
Ba	1695	1572	1866	3825	3976	55297	37466	1229	1697	1725	1345	3488	3988	5193
Th	5.80	342.33	362.58	23.00	34.86	41.55	27.25	33.94	32.46	28.56	32.50	26.49	107.08	80.47
U	1.77	23.87	26.92	2.99	6.55	2.60	1.46	7.41	6.30	6.03	5.84	4.53	7.19	8.75
Nb	7.09	148.94	187.67	44.96	53.76	12.20	7.95	59.21	55.71	55.71	55.11	36.95	54.05	12.06
Ta	0.23	2.30	2.75	1.16	1.29	0.35	0.61	2.52	2.30	2.31	2.33	1.51	3.41	1.15
Zr	106	1197	1413	176	256	0.66	1.36	381	290	298	271	390	352	396
Hf	2.35	16.56	19.43	3.16	4.67	0.66	0.43	7.76	6.07	6.52	6.02	7.02	11.55	11.15
Co	4.62	1.82	1.32	2.35	3.45	0.96	0.67	2.35	0.22	0.35	0.26	8.82	2.05	25.09
Ni	3.27	14.14	1.99	4.01	9.86	9.18	5.58	2.81	0.43	0.34	1.25	12.43	7.95	32.08
Cr	12.69	29.35	10.00	18.35	19.12	27.39	7.50	9.32	7.33	6.78	11.86	19.13	17.46	68.16
V	23.75	32.94	31.11	25.39	27.36	3.48	1.18	21.09	25.76	26.22	23.16	43.07	23.61	112.25
Sc	7.15	6.38	6.99	8.74	7.85	3.08	3.52	8.51	7.07	6.10	6.33	10.85	1.62	17.12
Cs	0.91	0.27	0.32	0.18	0.22	0.34	0.71	0.43	0.31	0.33	0.32	0.53	1.05	5.77
Ga	58.10	60.66	61.71	67.52	46.97	239.06	219.45	70.72	74.47	72.92	73.52	68.60	27.25	235.55
Cu	9.62	8.52	8.03	6.73	5.69	18.27	11.07	8.04	9.53	8.62	11.51	48.36	39.53	208.92
Pb	13.27	61.06	50.37	14.47	15.78	2374.56	121.32	30.43	34.73	42.65	46.68	31.32	47.46	26.92
Zn	36.49	99.67	104.08	37.83	73.80	856.10	40.44	118.26	53.12	33.90	56.07	85.28	85.33	360.15
Be	2.30	17.92	18.15	3.89	4.89	1.23	0.15	9.11	5.43	5.90	5.62	5.81	4.37	9.62
La	81.50	174.62	187.46	330.85	383.69	23164.39	18674.57	130.30	100.29	85.64	72.21	208.09	1446.48	7859.43
Ce	128.85	244.16	231.99	489.15	560.84	40390.16	36939.65	192.62	168.54	136.41	112.47	336.19	1687.38	9308.62
Pr	10.20	16.42	16.97	30.48	32.84	3016.81	2800.64	14.49	11.48	12.63	10.50	24.74	163.24	774.89
Nd	43.37	74.72	76.91	97.28	101.77	8811.86	7671.86	67.00	51.66	44.19	37.27	86.56	583.33	2473.67
Sm	4.78	8.64	8.78	13.91	13.26	838.34	544.55	8.73	6.91	5.24	4.92	13.85	69.01	206.97
Eu	1.38	2.23	2.29	4.15	3.94	136.96	109.51	2.02	1.67	1.38	1.32	4.29	16.98	35.69
Gd	3.58	7.52	7.73	13.43	13.04	733.01	570.27	6.98	5.44	4.17	4.18	12.46	44.15	104.89
Tb	0.26	0.70	0.73	1.03	1.00	62.38	45.65	0.71	0.56	0.45	0.49	1.13	5.42	13.48
Dy	0.83	3.08	3.21	3.36	3.25	137.42	86.28	3.14	2.47	2.17	2.48	4.34	22.22	18.03
Ho	0.14	0.64	0.70	0.58	0.84	18.60	12.29	0.64	0.50	0.44	0.51	0.78	4.11	5.11

(Continued on following page)

TABLE 2 (Continued) Whole-rock major and trace element compositions of the quartz syenite, REE ore samples, and altered rocks from Chishan and Longbaoshan REE deposits.

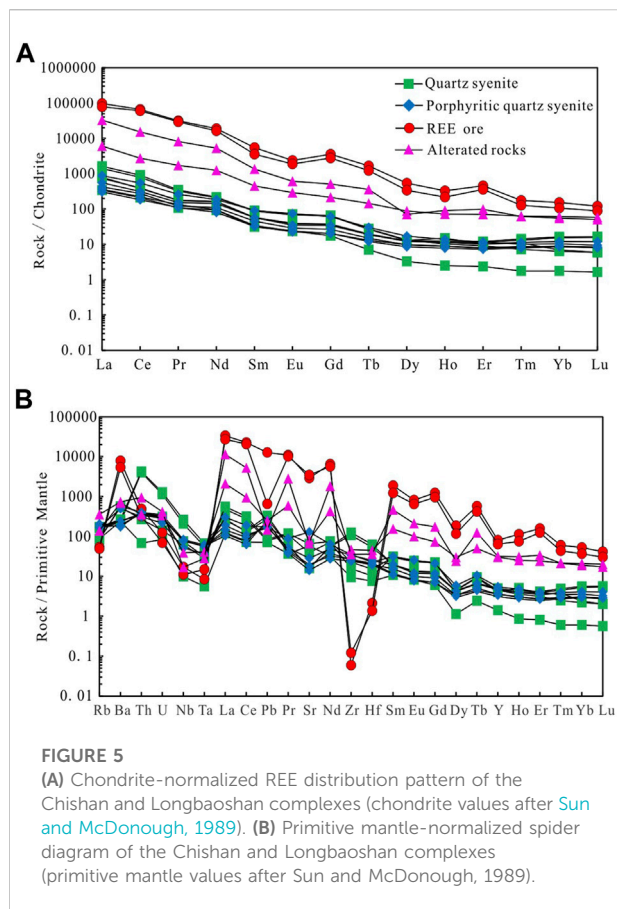
Sample number	18CS-01	18CS-10	18CS-11	18CS-12	18CS-33	18CS-05	18CS-18	LBS-01	LBS-04	LBS-06	LBS-07	LBS-09	P6D8h1	P6D8h3
Er	0.39	1.89	1.99	1.51	1.67	75.85	59.68	1.70	1.31	1.20	1.30	1.93	11.69	16.25
Tm	0.04	0.33	0.36	0.18	0.28	4.46	3.25	0.29	0.21	0.20	0.22	0.26	1.60	1.58
Yb	0.30	2.61	2.77	1.08	1.19	26.05	18.18	2.03	1.51	1.47	1.46	1.76	10.38	9.34
Lu	0.04	0.40	0.42	0.15	0.15	3.06	2.24	0.30	0.21	0.20	0.21	0.24	1.49	1.28
Y	6.44	21.15	22.93	20.51	18.35	366.08	290.98	21.71	16.01	14.24	16.35	24.79	138.79	144.60
∑REE	275.7	538.0	542.3	987.2	1117.8	77419.3	67538.6	440.1	358.2	301.7	255.2	702.4	4067.5	20829.2
LREE/HREE	18.1	19.1	17.6	21.4	17.2	17.3	19.1	28.9	28.0	28.3	29.4	28.1	39.3	121.6
La _N /Yb _N	32.0	41.7	35.6	31.5	23.5	23.1	29.0	72.2	69.8	69.4	77.7	70.5	99.9	603.5
δEu	0.97	0.82	0.83	0.92	0.91	0.52	0.60	0.77	0.80	0.87	0.86	0.98	0.88	0.66

*Note: The whole-rock major and trace element data of quartz syenite are obtained from previously published work (Wei et al., 2019).



listed in Table 2. The Chishan quartz syenite samples have SiO_2 contents of 69.02–71.72 wt%, Al_2O_3 contents of 13.51–16.12 wt%, and Na_2O , K_2O , and CaO contents of 5.53–7.13 wt%,

3.34–4.43 wt%, and 0.38–1.59 wt%, respectively. These samples are relatively high in SiO_2 , total alkali ($\text{Na}_2\text{O} + \text{K}_2\text{O}$) and Al_2O_3 and low in TiO_2 (0.06–0.17 wt%). These samples are mainly



classified as belonging to the alkaline series (Figure 4A), with an aluminum saturation index (A/CNK) of 0.83–0.98, showing a metaluminous to peralkaline characteristic (Figure 4B). They plot within the high-K field on the SiO₂ versus K₂O diagram (Figure 4C), mainly in the alkali-calcic field in the SiO₂ versus K₂O + Na₂O—CaO diagram (Figure 4D).

The Longbaoshan porphyritic quartz syenite samples have SiO₂ = 62.87–69.01 wt%, Al₂O₃ = 16.77–17.64 wt%, Na₂O = 6.61–6.89 wt%, K₂O = 5.02–5.21 wt%, and CaO = 0.16–1.49 wt%. On the total alkali versus silica (TAS) diagram (Figure 4A), the majority of these sample plots fall within the quartz monzonite field. As shown in the A/CNK versus A/NK diagram, these samples show a peraluminous to metaluminous affinity (Figure 4B). All the samples plot within the shoshonite field on the SiO₂ versus K₂O diagram (Figure 4C), and within the alkalic field on the SiO₂ versus K₂O + Na₂O—CaO diagram (Figure 4D).

The chondrite normalized REE patterns (Figure 5A) show that both the Chishan quartz syenite samples and Longbaoshan porphyritic quartz syenite samples show obvious REE fractionation and have the features of enrichment in light REEs (LREEs) and depletion in heavy REEs (HREEs). Moreover, they have similar REE components with total REE concentrations (ΣREE) of 255.2–1117.8 ppm, LREE/HREE ratios

of 17.2–29.4, (La/Yb)_N values of 23.5–77.7, and Eu anomalies (δEu) of 0.77–0.98. On the primitive mantle-normalized trace element spider diagram (Figure 5B), they are characterized by enrichment in large-ion lithophile elements (LILEs, e.g., Rb, Ba, and Sr), depletion in high field strength elements (HFSEs, e.g., Nb and Ta), and positive Pb anomalies and negative Nd and Dy anomalies.

The Chishan REE ores and Longbaoshan altered rocks are highly enriched in REEs (ΣREE = 4067.5–77419.3 ppm), with LREE/HREE ratios of 17.3–121.6 and (La/Yb)_N values of 23.1–603.5. In the chondrite-normalized REE patterns (Figure 5A), these samples exhibit distinct REE fractionation and features of enrichment in LREEs and depletion in HREEs with mild negative Eu (δEu = 0.52–0.88) anomalies. On the primitive mantle-normalized trace element spider diagram (Figure 5B), they are characterized by exceeding enrichment in LILEs (Rb and Ba), depletion in HFSEs (Nb, Ta, Zr, and Hf), and negative Pb and Dy anomalies.

4.3 Whole rock Sr–Nd–Pb isotopes

The Sr–Nd–Pb isotopic analysis results are listed in Table 3. The Chishan quartz syenite samples have uniform initial (⁸⁷Sr/⁸⁶Sr)_i ratios (0.7062–0.7088) and negative ε_{Nd}(t) values (–12.9 to –9.3), whereas the Longbaoshan porphyritic quartz syenite samples have high initial (⁸⁷Sr/⁸⁶Sr)_i ratios (0.7083–0.7100) and lower ε_{Nd}(t) values (–14.6 to –13.6). The Chishan REE ore samples have similar initial (⁸⁷Sr/⁸⁶Sr)_i ratios (0.7073–0.7077) and ε_{Nd}(t) values (–9.3 to –8.8) to the quartz syenite, and the Longbaoshan altered rocks also have similar initial (⁸⁷Sr/⁸⁶Sr)_i ratios (0.7087–0.7089) and ε_{Nd}(t) values (–13.3 to –13.1) to the porphyritic quartz syenite.

The Chishan quartz syenite samples and the Longbaoshan porphyritic quartz syenite samples have coincident Pb isotope compositions with the (²⁰⁶Pb/²⁰⁴Pb)_t, (²⁰⁷Pb/²⁰⁴Pb)_t, and (²⁰⁸Pb/²⁰⁴Pb)_t ratios of 17.25–17.63, 15.41–15.51, and 36.25–37.84, respectively. The Chishan REE ore samples and Longbaoshan altered rocks also have similar Pb isotope compositions to the (porphyritic) quartz syenite samples ((²⁰⁶Pb/²⁰⁴Pb)_t = 17.19 to 17.52, (²⁰⁷Pb/²⁰⁴Pb)_t = 15.44 to 15.53, and (²⁰⁸Pb/²⁰⁴Pb)_t = 36.99–37.81).

4.4 Zircon Hf isotopes

The *in situ* Hf isotopic analysis results of the (porphyritic) quartz syenite are listed in Table 4. The results show that they have analogical ε_{Hf}(t) values. In total, five zircon grains from sample 18CS-01 yield ε_{Hf}(t) values from –15.8 to –13.2 (mean = –14.4) and Hf model ages (T_{DM^C}) of 2.07–2.19 Ga

TABLE 3 Sr-Nd-Pb isotopic compositions of the quartz syenite, REE ore samples, and altered rocks from Chishan and Longbaoshan REE deposits.

Samples	18CS-01	18CS-10	18CS-11	18CS-12	18CS-33	18CS-05	18CS-18	LBS-01	LBS-04	LBS-06	LBS-07	LBS-09	P6D8h1	P6D8h3
Rb (ppm)	55	103	110	53	54	34	31	130	108	111	107	108	146	225
Sr (ppm)	1236	340	338	831	1381	61432	73381	598	372	416	297	2742	491	1407
⁸⁷ Rb/ ⁸⁶ Sr	0.044506	0.303209	0.325829	0.063802	0.039096	0.000553	0.000422	0.216465	0.290766	0.268058	0.360800	0.039409	0.297352	0.159915
⁸⁷ Sr/ ⁸⁶ Sr	0.708933	0.709161	0.709365	0.706476	0.706293	0.707704	0.707326	0.709185	0.710136	0.710079	0.710716	0.708466	0.709253	0.709229
2s	0.000007	0.000005	0.000007	0.000007	0.000007	0.000007	0.000007	0.000007	0.000005	0.000007	0.000006	0.000005	0.000007	0.000007
Sm (ppm)	4.78	8.64	8.78	13.91	13.26	838.34	544.55	8.73	6.91	5.24	4.92	13.85	69.01	206.97
Nd (ppm)	74.72	76.91	97.28	101.77	73.75	6397.63	19.19	8811.86	1539.23	1298.24	67.00	51.66	583.33	2473.67
¹⁴⁷ Sm/ ¹⁴⁴ Nd	0.110207	0.115629	0.114154	0.142984	0.130293	0.095138	0.07098	0.130289	0.133756	0.118573	0.132022	0.160013	0.118304	0.083669
¹⁴³ Nd/ ¹⁴⁴ Nd	0.511906	0.512078	0.512081	0.512094	0.512107	0.51208	0.512085	0.511871	0.511874	0.511879	0.511891	0.511862	0.511895	0.511874
2s	0.000004	0.000004	0.000005	0.000006	0.000006	0.000005	0.000005	0.000005	0.000005	0.000006	0.000006	0.000005	0.000004	0.000004
t (Ma)	126	126	126	126	126	126	126	124	124	124	124	124	124	124
(⁸⁷ Sr/ ⁸⁶ Sr) _i	0.708854	0.708622	0.708786	0.706363	0.706224	0.707703	0.707325	0.708804	0.709624	0.709607	0.710080	0.708397	0.708729	0.708947
ε _{Nd} (t)	-12.9	-9.6	-9.6	-9.8	-9.3	-9.3	-8.8	-13.9	-13.9	-13.6	-13.6	-14.6	-13.3	-13.1
t _{DM1} (Ma)	1830	1666	1636	2272	1904	1376	1139	2331	2426	2033	2344	3635	2002	1495
t _{DM2} (Ma)	1967	1702	1695	1712	1675	1672	1633	2048	2048	2020	2019	2101	1995	1983
²⁰⁶ Pb/ ²⁰⁴ Pb	16.2773	17.7739	18.1029	17.8867	18.0279	17.2471	17.2076	17.5402	17.6768	17.7527	17.427	17.633	17.5717	17.9221
²⁰⁷ Pb/ ²⁰⁴ Pb	15.1747	15.4568	15.4734	15.4361	15.4377	15.4486	15.4369	15.5013	15.5111	15.5169	15.4979	15.5219	15.5181	15.5523
²⁰⁸ Pb/ ²⁰⁴ Pb	36.2755	38.8985	39.3357	38.1085	38.1546	37.5938	37.899	37.8525	38.0413	38.1104	37.7826	37.9901	37.8748	38.9284
Pb (ppm)	13.27	61.06	50.37	14.47	15.78	2374.6	121.32	30.43	34.73	42.65	46.68	31.32	47.46	26.92
Th (ppm)	5.80	342.33	362.58	23.00	34.86	41.55	27.25	33.94	32.46	28.56	32.50	26.49	107.08	80.47
U (ppm)	1.77	23.87	26.92	2.99	6.55	2.60	1.46	7.41	6.30	6.03	5.84	4.53	7.19	8.75
(²⁰⁶ Pb/ ²⁰⁴ Pb) _t	17.3209	17.2863	17.4291	17.6314	17.5138	17.2458	17.1929	17.2464	17.4569	17.5809	17.2764	17.4579	17.3887	17.5217
(²⁰⁷ Pb/ ²⁰⁴ Pb) _t	15.4671	15.4331	15.4407	15.4237	15.4127	15.4485	15.4362	15.487	15.5004	15.5086	15.4906	15.5134	15.5092	15.5329
(²⁰⁸ Pb/ ²⁰⁴ Pb) _t	36.7078	36.6091	36.5848	37.4656	37.2588	37.5868	37.8093	37.4119	37.6703	37.8441	37.5083	37.6548	36.9826	37.7227

TABLE 4 Zircon Hf isotopic compositions of the quartz syenite from Chishan and Longbaoshan complexes.

Rock type	Spots	$^{176}\text{Yb}/^{177}\text{Hf}$	2σ	$^{176}\text{Lu}/^{177}\text{Hf}$	2σ	$^{176}\text{Hf}/^{177}\text{Hf}$	2σ	t (Ma)	$\epsilon_{\text{Hf}}(0)$	$\epsilon_{\text{Hf}}(t)$	$T_{\text{DM}}(\text{Ma})$	$T_{\text{DM}}^{\text{C}}(\text{Ma})$	$f_{\text{Lu/Hf}}$
Quartz syenite*	18CS-01-01	0.013407	0.000144	0.000586	0.000006	0.282297	0.000018	126	-16.8	-14.1	1334	2078	-0.98
	18CS-01-03	0.015576	0.000126	0.000718	0.000005	0.282282	0.000029	126	-17.3	-14.6	1359	2112	-0.98
	18CS-01-08	0.013584	0.000105	0.000573	0.000005	0.282248	0.000025	126	-18.5	-15.8	1400	2186	-0.98
	18CS-01-13	0.011379	0.000058	0.000519	0.000003	0.282322	0.000019	126	-15.9	-13.2	1296	2020	-0.98
	18CS-01-16	0.022202	0.000914	0.000943	0.000037	0.282299	0.000021	126	-16.7	-14.0	1343	2074	-0.97
Porphyritic quartz syenite	LBS-01-02	0.031167	0.000339	0.001094	0.000011	0.282287	0.000031	124	-17.2	-14.5	1365	2102	-0.97
	LBS-01-07	0.017183	0.000082	0.000660	0.000004	0.282291	0.000027	124	-17.0	-14.3	1344	2090	-0.98
	LBS-01-15	0.025887	0.000169	0.001168	0.000008	0.282306	0.000030	124	-16.5	-13.8	1342	2060	-0.96
	LBS-01-20	0.023971	0.000295	0.000908	0.000010	0.282228	0.000028	124	-19.2	-16.5	1440	2231	-0.97
	LBS-01-24	0.025287	0.000207	0.000986	0.000007	0.282191	0.000029	124	-20.5	-17.9	1495	2315	-0.97

Note: constants used in calculation: $(^{176}\text{Lu}/^{177}\text{Hf})_{\text{CHUR}}$, 0.0332, $(^{176}\text{Hf}/^{177}\text{Hf})_{\text{CHUR}, 0}$, 0.282772; $(^{176}\text{Lu}/^{177}\text{Hf})_{\text{DM}, 0}$, 0.0384, $(^{176}\text{Hf}/^{177}\text{Hf})_{\text{DM}, 0}$, 0.28325; constant $\lambda=1.867\times 10^{-11}\text{a}^{-1}$. * Note: The zircon Hf compositions of quartz syenite are obtained from previously published work (Wei et al., 2019).

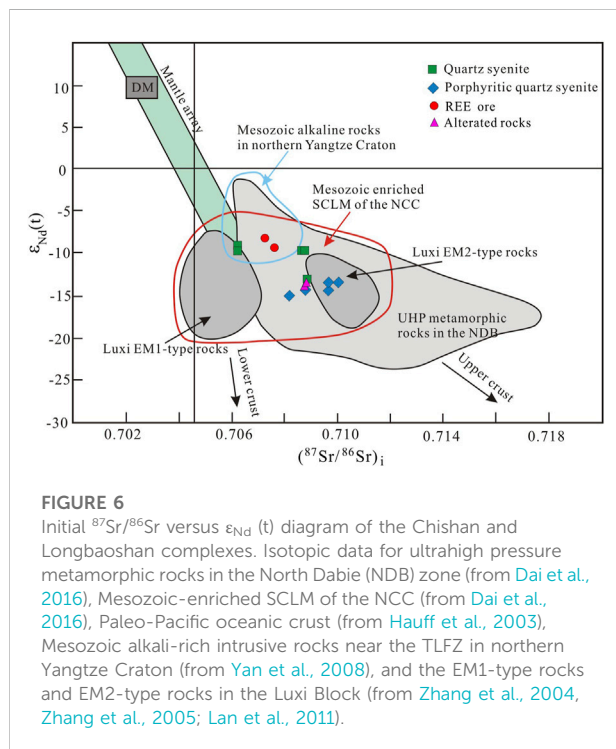


FIGURE 6

Initial $^{87}\text{Sr}/^{86}\text{Sr}$ versus $\epsilon_{\text{Nd}}(t)$ diagram of the Chishan and Longbaoshan complexes. Isotopic data for ultrahigh pressure metamorphic rocks in the North Dabie (NDB) zone (from Dai et al., 2016), Mesozoic-enriched SCLM of the NCC (from Dai et al., 2016), Paleo-Pacific oceanic crust (from Hauff et al., 2003), Mesozoic alkali-rich intrusive rocks near the TLFZ in northern Yangtze Craton (from Yan et al., 2008), and the EM1-type rocks and EM2-type rocks in the Luxi Block (from Zhang et al., 2004, Zhang et al., 2005; Lan et al., 2011).

(mean = 2.09 Ga). In total, five zircon grains from sample LBS-01 yield $\epsilon_{\text{Hf}}(t)$ values of -17.9 to -13.8 (mean = -15.4) and T_{DM}^{C} of 2.06–2.32 Ga (mean = 2.16 Ga).

5 Discussion

5.1 Timing of magmatism

The zircon grains from the (porphyritic) quartz syenite exhibit growing oscillatory zoning (Figures 3A,B), which coupled with relatively high Th/U ratios (>0.2 and 1.0) (Table 1), indicate a magmatic origin. Therefore, the weighted mean $^{206}\text{Pb}/^{238}\text{U}$ ages of 126.2 ± 1.1 Ma and 123.7 ± 0.7 Ma can represent the emplacement ages of the syenitic rocks from the Chishan and Longbaoshan complexes, respectively.

The emplacement age of the Chishan quartz syenite agreed with the previously reported ages (122–126 Ma) of the alkaline complex within the error range (Liang et al., 2017; Wei et al., 2019; Ding et al., 2022). However, the obtained diagenetic age (123.7 ± 0.7 Ma) of the porphyritic quartz syenite is slightly less than the precious reported poorly defined Rb–Sr isochron age (129.3 Ma, Zhang et al., 2005) and LA-ICP-MS zircon U–Pb ages (129.4–131.7 Ma, Lan et al., 2011) of the Longbaoshan complex. The slight difference between the ages of this study and those of predecessors indicates that the Longbaoshan complex was formed in a magmatic activity lasting relatively for a long duration.

Comparing the emplacement ages of the quartz syenite and porphyritic quartz syenite, it is found that they are both formed in the late Early Cretaceous. There is a broad consensus that the NCC has undergone large-scale lithospheric thinning or destruction since the late Paleozoic (Zhai et al., 2002; Deng

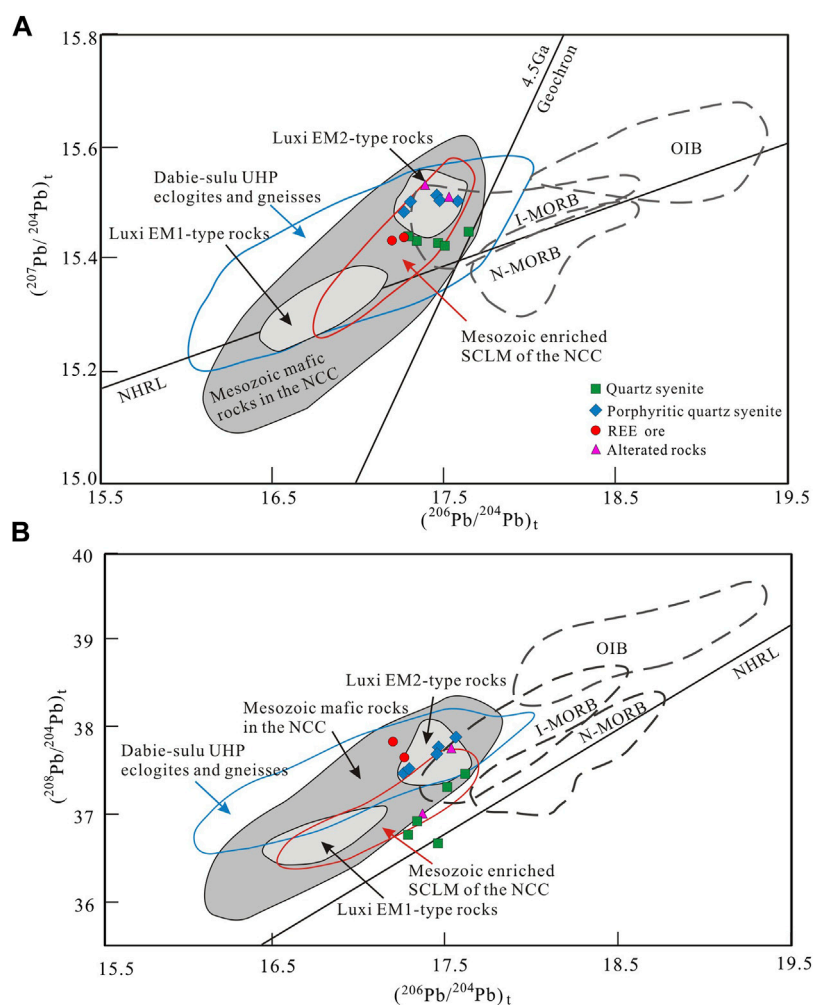


FIGURE 7

Diagrams of $^{207}\text{Pb}/^{204}\text{Pb}$ versus $^{206}\text{Pb}/^{204}\text{Pb}$ (A) and $^{208}\text{Pb}/^{204}\text{Pb}$ versus $^{206}\text{Pb}/^{204}\text{Pb}$ (B) for the Chishan and Longbaoshan complexes. Data are also plotted for Mesozoic-enriched SCLM of the NCC (from Dai et al., 2016), Dabie-Sulu UHP eclogites and gneisses (from Yang K. F. et al., 2012), Mesozoic mafic rocks in the NCC (from Li and Yang, 2003) and the EM1-type rocks and EM2-type rocks in the Luxi Block (from Zhang et al., 2005; Lan et al., 2011).

et al., 2003; Chen, 2010; Yang et al., 2018b), and the peak time of destruction and thinning was the Early Cretaceous (125–120 Ma) (Wu et al., 2005; Zhang et al., 2014; Zheng et al., 2018; Yang et al., 2020; Zhang et al., 2020; Zeng et al., 2022). Thus, the diagenesis time of the Chishan and Longbaoshan complexes is consistent with the peak period of the NCC destruction process.

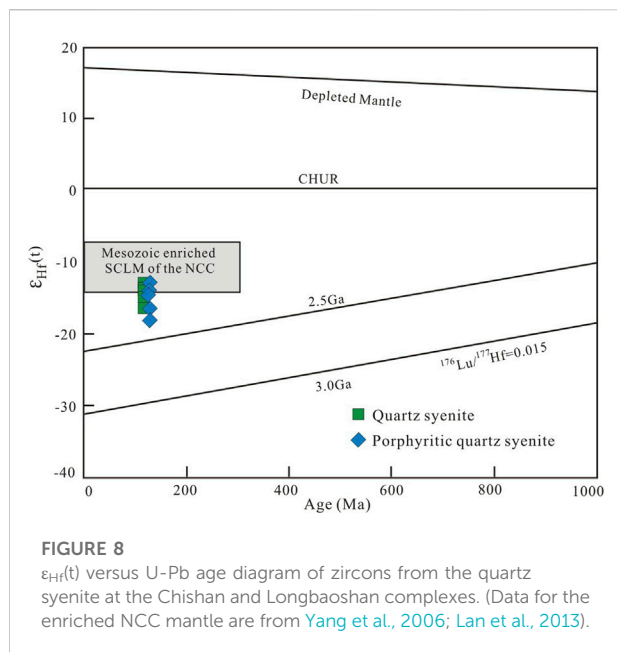
5.2 Petrogenesis

5.2.1 Magma source

The spatial isolated Chishan quartz syenite and Longbaoshan porphyritic quartz syenite have the similar diagenetic ages, chemical characteristics, Sr–Nd–Pb isotopic and zircon Hf isotopic compositions, and normalized trace

element and REE patterns, indicating that they may be of cognetic origin.

The Chishan quartz syenite samples and Longbaoshan porphyritic quartz syenite samples have similar chemical characteristics of relatively high alkalis ($\text{Na}_2\text{O} + \text{K}_2\text{O} = 7.62\text{--}10.94$ wt%), high potassium ($\text{Na}_2\text{O}/\text{K}_2\text{O} = 0.28\text{--}0.89$) and metaluminous ($A/\text{CNK} = 0.75\text{--}1.00$), and low TiO_2 content (0.06–0.17 wt%). In the SiO_2 versus K_2O diagram (Figure 4C), all the sample plots fall within the high-K and shoshonite fields. The rocks display peraluminous to peralkaline features in the A/CNK versus A/NK diagram (Figure 4B). In the SiO_2 versus $\text{K}_2\text{O} + \text{Na}_2\text{O} - \text{CaO}$ diagram (Figure 4D), all the sample plots fall within the alkalic and alkali-calcic fields. Therefore, they have the obvious characteristics of alkaline and metaluminous rocks.



The syenitic rocks from the Chishan and Longbaoshan complexes show similar REE and trace element patterns (Figure 5 and Table 2) with the characteristics of enrichment in LREEs and LILEs (Rb, Ba, Pb, and K) and depletion in HFSEs (Ti, Nb, and Ta), along with a slight negative Eu anomaly (Figure 5B). The chondrite-normalized REE patterns also display strongly fractionated LREE/HREE patterns (Figure 5A). Those chemical characteristics are almost the same as the mantle-derived mafic intrusions and volcanics in southeastern NCC during the Early Cretaceous (Zhang et al., 2002; Zhang et al., 2005; Lan et al., 2011).

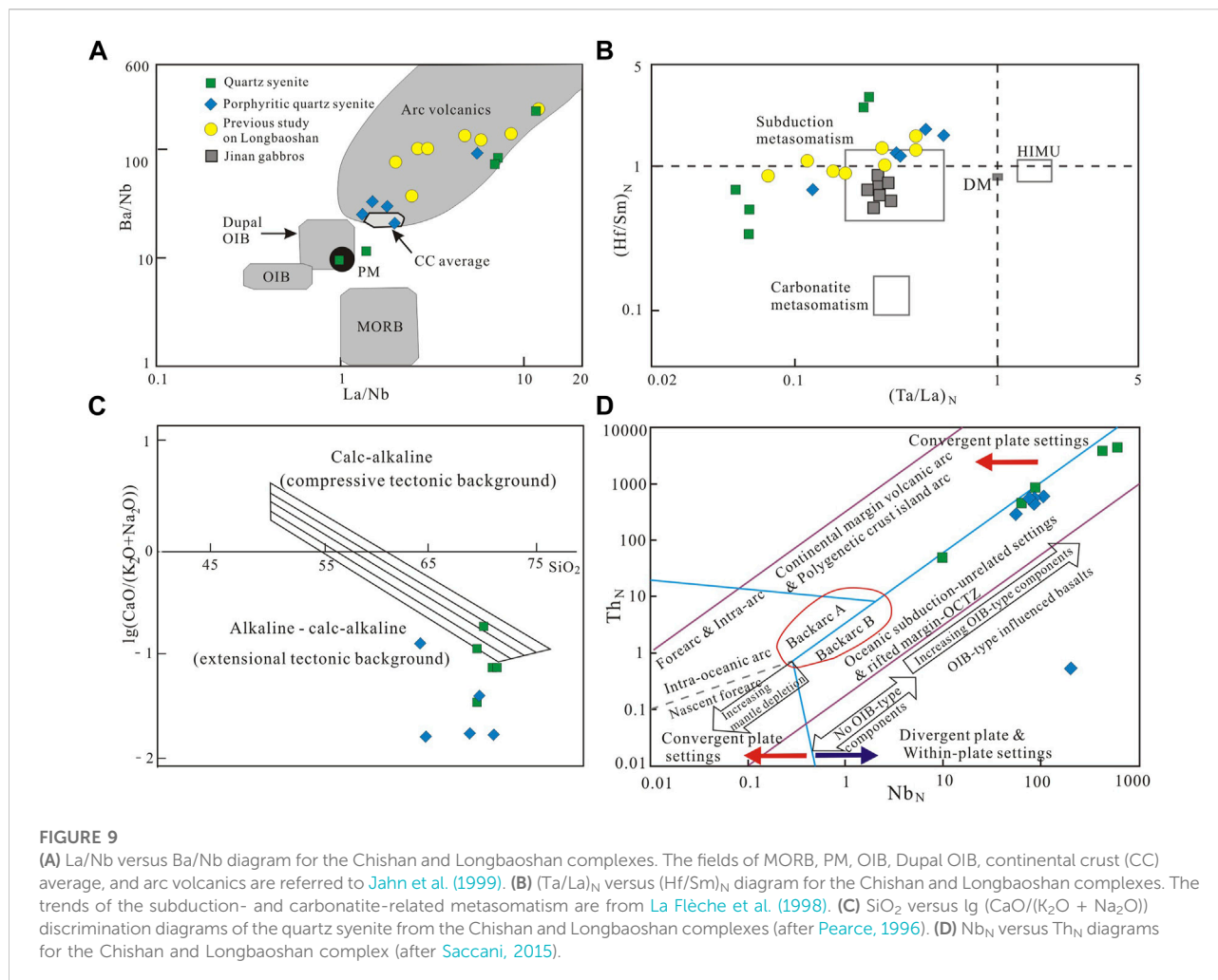
The Chishan quartz syenite samples and Longbaoshan porphyritic quartz syenite samples have high initial $^{87}\text{Sr}/^{86}\text{Sr}$ ratios and low $\epsilon_{\text{Nd}}(t)$ values ($(^{87}\text{Sr}/^{86}\text{Sr})_i = 0.7062$ to 0.7100 and $\epsilon_{\text{Nd}}(t) = -14.6$ to -9.3), which are characteristics of the EM2-like character (Zhang et al., 2005; Lan et al., 2011). In the $\epsilon_{\text{Nd}}(t) - (^{87}\text{Sr}/^{86}\text{Sr})_i$ diagram (Figure 6), all the sample plots fall near the mantle array despite the variations and fall within the subcontinental lithospheric mantle (SCLM), also suggesting a mantle origin. The (porphyritic) quartz syenite samples have low $(^{206}\text{Pb}/^{204}\text{Pb})_i$ (17.2–17.6), slightly high $(^{207}\text{Pb}/^{204}\text{Pb})_i$ ($\Delta 7/4 = 15.4$ – 15.5), and very high $(^{208}\text{Pb}/^{204}\text{Pb})_i$ ($\Delta 8/4 = 36.5$ – 37.8) (Table 3 and Figure 7), similar to the I-MORB and EM2-type rocks (Zhang et al., 2002; Zhang et al., 2005). In the Pb isotopic diagrams (Figure 7), majority of sample plots fall within the Mesozoic mafic rock field, suggesting that they have similar characteristics to the Mesozoic basalts and mafic intrusive rocks in the NCC (Zhang et al., 2002; Zhang et al., 2004). In addition, the (porphyritic) quartz syenite samples have similar $(^{176}\text{Hf}/^{177}\text{Hf})_i$ and $\epsilon_{\text{Hf}}(t)$ values (0.28219 to 0.28232 and -17.9 to -13.2 , respectively) (Table 4), and in the

Hf isotope diagram (Figure 8), all the sample plots fall above the 2.5 Ga continental crust evolutionary line, as well as within the Mesozoic enriched SCLM field. Thus, it is reasonable to deduce that the (porphyritic) quartz syenites were derived predominantly from enriched lithospheric mantle (EM2-type).

Previous studies have revealed that the mafic intrusions and volcanic rocks that formed in the Early Cretaceous in southeastern NCC were originated from a mantle domain of arc-like and isotopically enriched (Wu et al., 2017; Dai et al., 2019; Ding et al., 2022). The (porphyritic) quartz syenite samples are characterized by low Nb/Th (0.52–1.95), Nb/La (0.09–0.85) ratios, relatively higher La/Nb (1.00–26.76), Th/Ta (12.39–148.65), Ba/Nb (9.90–239.12) ratios, and negative Nb–Ta anomalies, which are similar to the sub-continental mantle-derived magma contaminated with crustal material (Santosh et al., 2016; Yang et al., 2018b). Moreover, this is also well-demonstrated by the Nd and zircon Hf model ages ($t_{\text{DM}2}$ of 1633–2048 Ma and T_{DM^C} from 2060 Ma to 2315 Ma, Tables 3, 4), which indicates variable proportions of the Paleoproterozoic crustal material. The crustal source is predominantly a reworked Paleoproterozoic crustal zone originating from the Yangtze Craton (Deng et al., 2018). In the La/Nb versus Ba/Nb diagram (Figure 9A), most of the syenitic sample plots fall within the arc volcanic field, indicative of the similar mantle source of the subducted mantle wedge (Lan et al., 2011). Furthermore, these samples have high $(\text{Hf}/\text{Sm})_N$ and relative low $(\text{Ta}/\text{La})_N$ ratios which are identical to the Jinan gabbros in the Luxi Block (Figure 9B), suggesting that this enriched mantle source may be related to subduction metasomatism (Lan et al., 2011). In addition, these isotopic compositions of the (porphyritic) quartz syenite are consistent with the Fangcheng basalts and mafic rocks in this region, which were considered to be originated from a lithospheric mantle highly reformed by subducted crust melts (Zhang et al., 2002; Xu et al., 2004; Yang K. F. et al., 2012). Thus, we propose that the (porphyritic) quartz syenites are also derived from lithospheric mantle, which is reformed by the SCLM melts.

5.2.2 Genetic model and process

Three models have been suggested for the generation of syenitic rocks: 1) partial melting of crustal rocks (Miyazaki et al., 2000; Martin, 2006) or an over-thickened crust (Tchameni et al., 2001); 2) partial melting of the enriched mantle or metasomatized mantle (Litvinovsky et al., 2002) or differential evolution of alkalic basaltic magma (Macdonald and Scaillet, 2006); 3) mixing of silica-undersaturated alkaline or mafic magmas derived from the mantle with granitic magmas derived from the lower crust (Zhao et al., 1995; Jung et al., 2007). Based on the aforementioned discussion, we consider that the origin of the (porphyritic) quartz syenite from the Chishan and Longbaoshan complexes should follow the second model. They derived from the lithospheric mantle converted by SCLM melts.



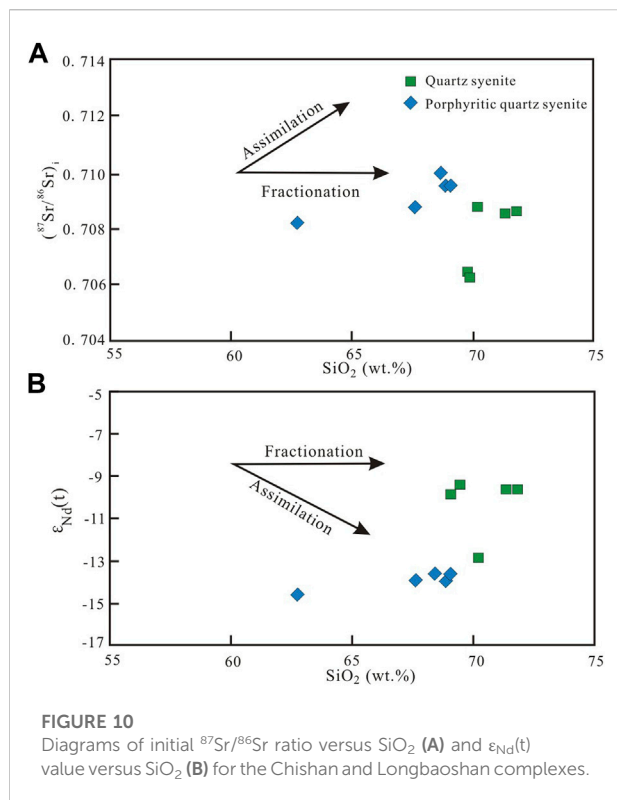
However, for the rocks formed by partial melting in the mantle source area, two main mechanisms have been proposed to reveal the reformation of lower crust materials: 1) the direct transformation of the magma source area by delaminated continental crust materials; 2) the assimilation or contamination of the crustal materials in the magma ascending process ([Yang D. B. et al., 2012](#)). In the $\epsilon_{\text{Nd}}(t)$ -SiO₂ and $(^{87}\text{Sr}/^{86}\text{Sr})_i$ -SiO₂ diagrams ([Figure 10](#)), the initial $^{87}\text{Sr}/^{86}\text{Sr}$ ratios and $\epsilon_{\text{Nd}}(t)$ values have no significant changes with the increase of SiO₂ contents, which is consistent with the evolution trend of fractional crystallization, manifesting that the assimilation of continental crust materials may have occurred principally in the magma chamber ([Zhang et al., 2005](#); [Lan et al., 2011](#)). Therefore, we conclude that the alkaline magma derived from the enriched lithospheric mantle was unevenly assimilated by melts derived from the continental crust in the magma chamber and then produced the parent magma of the (porphyritic) quartz syenites.

Through the aforementioned discussion, the formation process of the (porphyritic) quartz syenite can be summarized as follows: before 130 Ma, the lithospheric mantle under the southeastern part of the Luxi Block reformed by the SCLM melts

and transformed from EM1-type into EM2-type in response to the subduction of the Yangtze continental crust ([Figure 11A](#)) ([Zhang et al., 2002](#), [Zhang et al., 2004](#); [Lan et al., 2011](#)). At ~130 Ma, due to subduction of the Paleo-Pacific plate, the converted EM2-type lithospheric mantle was partially melted and produced potassium-rich alkaline magma marked by enrichment of LREEs and LILEs and depletion of HFSEs ([Figure 11B](#)) ([Zhang et al., 2002](#); [Zhang et al., 2004](#), [Zhang et al., 2005](#)). This magma assimilated the crust-derived melts and were up-invaded with the lithospheric thinning and asthenosphere mantle upwelling, forming the Chishan and Longbaoshan alkaline complexes ([Figure 11C](#)).

5.3 Tectonic setting

All the studied syenitic rocks from the Chishan and Longbaoshan complexes have an arc-like affinity with enriched LREEs and LILEs (e.g., Ba and Th) and depleted HFSE (e.g., Nb and Ta). This can be further evidenced by the



La/Nb versus Ba/Nb diagram (Figure 9A), in which most syenitic samples plot within the arc volcanic field. In addition, the high $(\text{Hf}/\text{Sm})_{\text{N}}$ and low $(\text{Ta}/\text{La})_{\text{N}}$ ratios (Figure 9B) of these samples suggest that the enriched mantle source may be associated with subduction metasomatism (La Flèche et al., 1998; Lan et al., 2011). Nevertheless, it is noteworthy that the syenitic samples plot within the extensional alkaline-calc-alkaline field in the Ig $(\text{CaO}/(\text{K}_2\text{O} + \text{Na}_2\text{O}))$ versus SiO_2 discrimination diagram (Figure 9C) and plot within the fields of divergent plate and within-plate settings in the Nb_{N} versus Th_{N} discrimination diagram (Figure 9D), implying an extensional tectonic setting (Wei et al., 2019; Ding et al., 2022). Moreover, the paleostress regimes reconstructed results of the Jiaolai Basin based on the effective fault-slip data and fold hinge data inversion showed that it has experienced E–W extension (135–121 Ma) and NW–SE extension (120–93 Ma) since the Cretaceous (Zhang et al., 2020). The study on the structural geology, paleomagnetism, and gravity modeling of Fengjiayu–Xibailianyu and Gubeikou plutons revealed that the NCC was also in a NW–SE trending extensional tectonics during 130–110 Ma with severe extension after ca. 127 Ma (Zeng et al., 2022).

Numerous studies have shown that the NCC was in an extensional tectonic environment during the Mesozoic and underwent craton destruction and extensive lithospheric thinning indicated by intense magmatism (Zhai et al., 2002; Deng et al., 2003; Yang et al., 2007). It has already been confirmed that the Early Cretaceous was a peak period for NCC destruction

and lithospheric thinning (Wu et al., 2005; Zheng, 2009; Goss et al., 2010) due to the rollback and retreat of subducting the Paleo-Pacific plate (Santosh, 2010; Zhu et al., 2012). In the early Mesozoic, the Paleo-Pacific plate subducted in a low angle along the continental margin of the eastern NCC and showed an important impact on the destruction and thinning of the latter continental lithosphere (Xu et al., 2012; Zheng et al., 2018; Zhu and Xu, 2019). It has been proposed that the angle of subduction gradually increased with the rollback and retreat of the subduction zone during the Early Cretaceous (Zhu and Xu, 2019). The transition of subduction angle may have occurred at ca. 140 Ma (Wu et al., 2005; Zhang et al., 2014; Zhao et al., 2017). In addition, partial melting of the SCLM as well as the destruction and extension of the lithosphere was also caused during this process (Zhu et al., 2012; Yang et al., 2021).

5.4 Relationship between quartz syenite and REE mineralization

It is widely accepted that REE mineralization is genetically relevant to mantle-derived carbonatite-alkaline magmatism (Goodenough et al., 2016; Smith et al., 2016; Liu et al., 2019; Fan et al., 2020; Xie et al., 2020). At Chishan and Longbaoshan, the REE mineralization generally occurred within quartz syenite and porphyritic quartz syenite, which were under the control of NW- and NE-trending faults and NNE- and NE-trending faults, respectively. Precisely published Rb–Sr isochron ages and ^{40}Ar – ^{39}Ar and U–Th dating results have yielded ages of 110–124 Ma of the REE mineralization (Tian et al., 2002; Lan et al., 2011; Ding et al., 2022), which are generally consistent with diagenetic ages of the syenitic rocks in this study. Actually, this age difference is basically consistent with the age error for magmatic hydrothermal deposits (Li et al., 1992; Tan et al., 2006). This spatial and temporal distribution consistency of the syenitic rocks and REE indicates that the mineralization has a certain genetic relationship with these alkaline rocks (Tian et al., 2002; Yu et al., 2010, 2014; Lan et al., 2011; Wei et al., 2019).

The aforementioned conclusions are also demonstrated by the geochemical and Sr–Nd–Pb isotopic characteristics of the syenitic rocks, REE ores, and altered rocks. The Chishan REE ores and Longbaoshan altered rocks are characterized by enrichment of LREEs and LILEs and depletion of HFSEs, which is similar to those of the syenitic rocks. From the chondrite-normalized REE patterns (Figure 5A), it can be seen that the REE distribution curve shapes of the Chishan REE ores and Longbaoshan altered rocks are basically similar to those of syenitic rocks. They all show a right-inclined distribution pattern, indicating that they have the characteristics of evolutionary inheritance. Furthermore, the Chishan REE ores and Longbaoshan altered rocks have similar Sr–Nd–Pb isotopic compositions to the syenitic rocks (Table 3; Figures 6, 7), indicating that the Chishan REE ores and

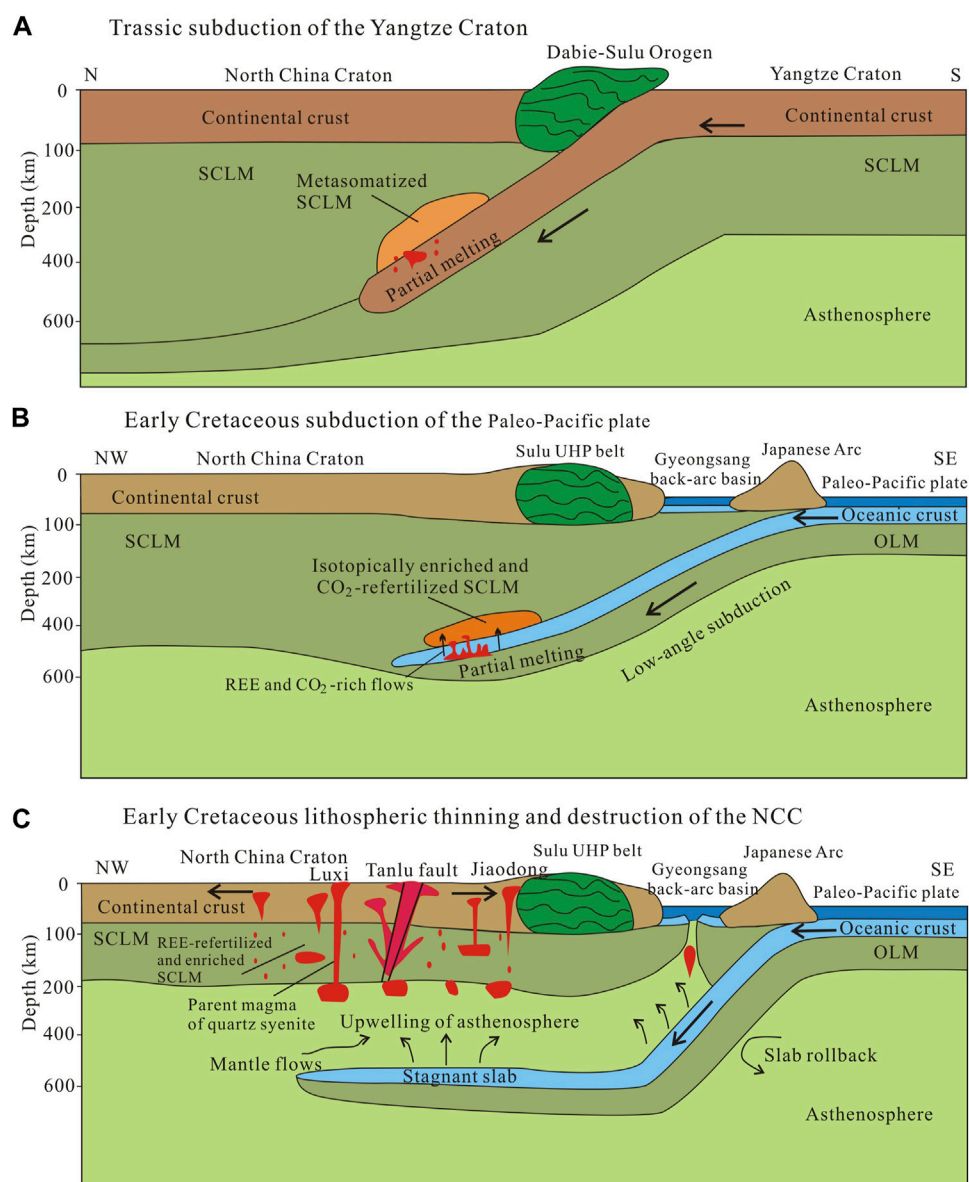


FIGURE 11

Simplified genetic model cross-sections of quartz syenite (modified after Zhu and Xu, 2019; Deng et al., 2020; Ding et al., 2022). (A) Trassic subduction of the Yangtze Craton. (B) Early Cretaceous subduction of the Paleo-Pacific plate. (C) Early Cretaceous lithospheric thinning and destruction of the NCC.

Longbaoshan altered rocks have identical material sources with the syenitic rocks which were originated from the enriched mantle. Moreover, the *in situ* Nd isotopic compositions from single minerals of bastnasite and monazite at the Chishan REE deposit also suggested that the REE was derived from the enriched lithospheric mantle (Lan et al., 2011), which is also identical to that of the syenitic rocks.

Some studies have shown that the sources of ore-forming materials of Bayan Obo and Maoniuping REE deposits are closely related to those of the enriched mantle (Hou et al., 2009; Xie et al.,

2009; Yang et al., 2009), indicating that the enriched mantle should be the source area of REE deposits. It has been suggested that melt-enriched LREE were derived from an enriched mantle metasomatized by REE- and CO₂-rich fluids that were released from subducted marine sediments (Walter et al., 2008; Yang et al., 2011; Hou et al., 2015; Liu et al., 2015; Ding et al., 2022).

In summary, based on the similar diagenetic/metallogenic ages, Sr–Nd–Pb isotopic compositions, and direct coexistence in space, we propose that the REE minerals have a genetic relationship with the syenitic rocks and they are homologous

products, and the mineralization shows inheritance to the magmatic hydrothermal evolution.

6 Conclusion

- 1) LA-ICP-MS zircon U-Pb dating indicated that the diagenetic ages of the Chishan quartz syenite and Longbaoshan porphyritic quartz syenite were 126.2 ± 1.1 Ma and 123.7 ± 0.7 Ma, respectively, which belong to the Early Cretaceous and correspond to the peak period for NCC destruction and lithospheric thinning.
- 2) Geochemical and Sr–Nd–Pb–Hf isotopic characteristics suggest that the Chishan quartz syenite and Longbaoshan porphyritic quartz syenite have the identical material source of an EM-2 type lithospheric mantle that was modified by SCLM melts while the Yangtze block subducted.
- 3) The Chishan quartz syenite and Longbaoshan porphyritic quartz syenite show an arc affinity, implying in an extensional tectonic setting associated with rollback and retreat of the subducting Paleo-Pacific plate.
- 4) Based on the similar diagenetic/metallogenic ages, Sr–Nd–Pb isotopic compositions, and direct coexistence in space, we propose that the quartz syenite and the REE ore-forming material are homologous products. The REE mineralization shows inheritance to the magmatic hydrothermal evolution.

Data availability statement

The original contributions presented in the study are included in the article/Supplementary Material; further inquiries can be directed to the corresponding authors.

Author contributions

PW, DL, and ZS conceived this research. PW wrote the manuscript and prepared the figures. DL, ZS, and KG reviewed and edited the draft. QL, KG, YZ, and CD participated in field

investigation. ZL, NC, WX, and CZ analyzed the data. All authors finally approved the manuscript and thus agreed to be accountable for this work.

Funding

This study was financially supported by the National Natural Science Foundation of China (Grant Nos. 42272104, 42172094, 41372086, 41672084, and 41772076), Natural Science Foundation of Shandong Province (Grant Nos. ZR2020QD028, ZR2020QD031, ZR2018QD002, and ZR2020MD032), Geological Exploration Project of Shandong Province (Grant Nos. LKZ (2020) 7, LKZ (2021) 7, LKZ (2022) 9), and a special fund for “Taishan scholars” project in the Shandong province.

Acknowledgments

We would like to express our thanks to the reviewers who offered constructive and valuable comments to improve the manuscript.

Conflict of interest

The authors declare that the research was conducted in the absence of any commercial or financial relationships that could be construed as a potential conflict of interest.

Publisher's note

All claims expressed in this article are solely those of the authors and do not necessarily represent those of their affiliated organizations, or those of the publisher, the editors, and the reviewers. Any product that may be evaluated in this article, or claim that may be made by its manufacturer, is not guaranteed or endorsed by the publisher.

References

- Blichert-Toft, J., and Albarède, F. (1997). The Lu–Hf isotope geochemistry of chondrites and the evolution of the mantle–crust system. *Earth Planet. Sci. Lett.* 148 (1–2), 243–258. doi:10.1016/S0012-821X(97)00040-X
- Bonin, B., Azzouni-Sekkal, A., Bussy, F., and Ferrag, S. (1998). Alkali–calcic and alkaline post-orogenic (PO) granite magmatism: Petrologic constraints and geodynamic settings. *Lithos* 45, 45–70. doi:10.1016/S0024-4937(98)00025-5
- Chen, B., Zhai, M. G., and Tian, W. (2007). Origin of the mesozoic magmatism in the north China craton: Constraints from petrological and geochemical data. *Geol. Soc. Lond. Spec. Publ.* 280, 131–151. doi:10.1144/SP280.6
- Chen, L. (2010). Concordant structural variations from the surface to the base of the upper mantle in the North China Craton and its tectonic implications. *Lithos* 120 (1–2), 96–115. doi:10.1016/j.lithos.2009.12.007
- Dai, F. Q., Zhao, Z. F., Zheng, Y. F., and Dai, L. Q. (2016). Slab–Mantle interaction in the petrogenesis of andesitic magmas: Geochemical evidence from postcollisional intermediate volcanic rocks in the Dabie orogen, China. *J. Petrol.* 57, 1109–1134. doi:10.1093/petrology/egw034
- Dai, F. Q., Zhao, Z. F., Zheng, Y. F., and Sun, G. C. (2019). The geochemical nature of mantle sources for two types of Cretaceous basaltic rocks from Luxi and Jiaodong in east-central China. *Lithos* 344–345, 409–424. doi:10.1016/j.lithos.2019.07.007

- Deng, J., Wang, C. M., Bagas, L., Santosh, M., and Yao, E. Y. (2018). Crustal architecture and metallogenesis in the south-eastern North China Craton. *Earth. Sci. Rev.* 182, 251–272. doi:10.1016/j.earscirev.2018.05.001
- Deng, J., Yang, L. Q., Groves, D. I., Zhang, L., Qiu, K. F., and Wang, Q. F. (2020). An integrated mineral system model for the gold deposits of the giant Jiaodong province, eastern China. *Earth. Sci. Rev.* 208, 103274. doi:10.1016/j.earscirev.2020.103274
- Deng, J., Yang, L. Q., Sun, Z. S., Wang, J. P., Wang, Q. F., Xin, H. B., et al. (2003). A metallogenic model of gold deposits of the Jiaodong granite-greenstone belt. *Acta Geol. Sin.-Engl.* 77 (4), 537–546. doi:10.1111/j.1755-6724.2003.tb00134.x
- Ding, C. W., Zhao, B. C., Dai, P., Li, D. P., Zhang, Z. L., Sun, R. T., et al. (2022). Geochronology, geochemistry and Sr-Nd-Pb-Hf isotopes of the alkaline-carbonatite complex in the Weishan REE deposit, Luxi Block: Constraints on the Genesis and tectonic setting of the REE mineralization. *Ore Geol. Rev.* 147, 104996. doi:10.1016/j.oregeorev.2022.104996
- Fan, H. R., Niu, H. C., Li, X. C., Yang, K. F., Yang, Z. F., and Wang, Q. W. (2020). The types, ore Genesis and resource perspective of endogenic REE deposits in China. *Chin. Sci. Bull.* 65, 3778–3793. (in Chinese with English abstract). doi:10.1360/TB-2020-0432
- Fan, W. M., Zhang, H. F., Baker, J., Jarvis, K. E., Mason, P. R. D., and Menzies, M. A. (2000). On and off the north China craton: Where is the archaean keel? *J. Petrol.* 41, 933–950. doi:10.1093/ptrology/41.7.933
- Frost, B. R., Barnes, C. G., Collins, W. J., Arculus, R. J., Ellis, D. J., and Frost, C. D. (2001). A geochemical classification for granitic rocks. *J. Petrol.* 42 (11), 2033–2048. doi:10.1093/ptrology/42.11.2033
- Gao, S., Rudnick, R. L., Xu, W. L., Yuan, H. L., Liu, Y. S., Walker, R. J., et al. (2008). Recycling deep cratonic lithosphere and generation of intraplate magmatism in the North China Craton. *Earth Planet. Sci. Lett.* 270, 41–53. doi:10.1016/j.epsl.2008.03.008
- Gao, S., Rudnick, R. L., Carlson, R. W., Mc Donough, W. F., and Liu, Y. S. (2002). Re-Os evidence for replacement of ancient mantle lithosphere beneath the North China Craton. *Earth Planet. Sci. Lett.* 198, 307–322. doi:10.1016/S0012-821X(02)00489-2
- Geng, J. Z., Li, H. K., Zhang, J., Zhou, H. Y., and Li, H. M. (2011). Zircon Hf isotope analysis by means of LA-MC-ICP-MS. *Geol. Bull. China* 30 (10), 1508–1513. (in Chinese with English abstract).
- Goldfarb, R. J., and Santosh, M. (2014). The dilemma of the jiaodong gold deposits: Are they unique? *Geosci. Front.* 5, 139–153. doi:10.1016/j.gsf.2013.11.001
- Goodenough, K. M., Schilling, J., Jonsson, E., Kalvig, P., Charles, N., Tuduri, J., et al. (2016). Europe's rare Earth element resource potential: An overview of REE metallogenetic provinces and their geodynamic setting. *Ore Geol. Rev.* 72, 838–856. doi:10.1016/j.oregeorev.2015.09.019
- Goss, S. C., Wilde, S. A., Wu, F., and Yang, J. (2010). The age, isotopic signature and significance of the youngest mesozoic granitoids in the jiaodong terrane, shandong province, north China craton. *Lithos* 120, 309–326. doi:10.1016/j.lithos.2010.08.019
- Griffin, W. L., Pearson, N. J., Belousova, E., Jackson, S. E., Van Acherbergh, E., O'Reilly, S. Y., et al. (2000). The Hf isotope composition of cratonic mantle: LAM-MC-ICPMS analysis of zircon megacrysts in kimberlites. *Geochim. Cosmochim. Acta* 64 (1), 133–147. doi:10.1016/S0016-7037(99)00343-9
- Griffin, W. L., Wang, X., Jackson, S. E., Pearson, N. J., O'Reilly, S. Y., Xu, X. S., et al. (2002). Zircon chemistry and magma mixing, SE China: *In-situ* analysis of Hf isotopes, tonglu and pingtan igneous complexes. *Lithos* 61 (3–4), 237–269. doi:10.1016/S0024-4937(02)00082-8
- Hauff, F., Hoernle, K., and Schmidt, A. (2003). Sr-Nd-Pb composition of Mesozoic Pacific oceanic crust (Site 1149 and 801, ODP Leg 185): Implications for alteration of ocean crust and the input into the Izu-Bonin-Mariana subduction system. *Geochem. Geophys. Geosyst.* 4, 8913. doi:10.1029/2002gc000421
- Hou, Z. Q., Liu, Y., Tian, S. H., Yang, Z. M., and Xie, Y. L. (2015). Formation of carbonate-related giant rare-Earth-element deposits by the recycling of marine sediments. *Sci. Rep.* 5 (1), 10231–10310. doi:10.1038/srep10231
- Hou, Z. Q., Tian, S. H., Xie, Y. L., Yang, Z. S., Yuan, Z. X., Yin, S. P., et al. (2009). The Himalayan Mianning-Dechang REE belt associated with carbonatite-alkaline complexes, eastern Indo-Asian collision zone, SW China. *Ore Geol. Rev.* 36 (1–3), 65–89. doi:10.1016/j.oregeorev.2009.03.001
- Irvine, T. N., and Baragar, W. R. A. (1971). A guide to the chemical classification of the common volcanic rocks. *Can. J. Earth Sci.* 8, 523–548. doi:10.1139/e71-055
- Jahn, B. M., Wu, F. Y., Lo, C. H., and Tsai, C. H. (1999). Crust-mantle interaction induced by deep subduction of the continental crust: Geochemical and Sr-Nd isotopic evidence from post-collisional mafic-ultramafic intrusions of the northern Dabie complex, central China. *Chem. Geol.* 157, 119–146. doi:10.1016/S0009-2541(98)00197-1
- Jung, S., Hoffer, E., and Hoernes, S. (2007). Neo-proterozoic rift-related syenites (northern damara belt, Namibia): Geochemical and Nd-Sr-Pb-O isotope constraints for mantle sources and petrogenesis. *Lithos* 96, 415–435. doi:10.1016/j.lithos.2006.11.005
- La Flèche, M. R., Camire, G., and Jenner, G. A. (1998). Geochemistry of post-acadian, carboniferous continental intraplate basalts from the maritimes basin, magdalen islands, quebec, Canada. *Chem. Geol.* 148, 115–136. doi:10.1016/s0009-2541(98)00002-3
- Lan, T. G., Fan, H. R., Hu, F. F., Tomkins, A. G., Yang, K. F., and Liu, Y. (2011). Multiple crust-mantle interactions for the destruction of the North China craton: Geochemical and Sr-Nd-Pb-Hf isotopic evidence from the longbaoshan alkaline complex. *Lithos* 122 (1–2), 87–106. doi:10.1016/j.lithos.2010.12.001
- Lan, T. G., Fan, H. R., Santosh, M., Hu, F. F., Yang, K. F., Yang, Y. H., et al. (2013). Crust-mantle interaction beneath the Luxi block, eastern North China craton: Evidence from coexisting mantle-and crust-derived enclaves in a quartz monzonite pluton. *Lithos* 177, 1–16. doi:10.1016/j.lithos.2013.05.017
- Li, C. J., Xu, B. T., Jiang, X. L., and Hu, Y. H. (1992). Time interval between the formation of host rock and the mineralization in some hydrothermal deposits of Southeast China with a discussion on some related problems. *Mineral. Deposits* 11 (2), 106–112+105. (in Chinese with English abstract).
- Li, S. G., Xiao, Y. L., Liou, D. L., Chen, Y. Z., Ge, N. J., Zhang, Z. Q., et al. (1993). Collision of the north China and yangtse blocks and formation of coesite-bearing eclogites: Timing and processes. *Chem. Geol.* 109, 89–111. doi:10.1016/0009-2541(93)90063-o
- Li, S. G., and Yang, W. (2003). Decoupling of surface and subsurface sutures in the Dabie orogen and a continent-collisional lithospheric-wedging model: Sr-Nd-Pb isotopic evidences of Mesozoic igneous rocks in eastern China. *Chin. Sci. Bull.* 48, 831–838. doi:10.1360/01wd0554
- Li, S. R., and Santosh, M. (2017). Geodynamics of heterogeneous gold mineralization in the North China Craton and its relationship to lithospheric destruction. *Gondwana Res.* 50, 267–292. doi:10.1016/j.gr.2017.05.007
- Liang, Y. W., Lai, Y., Hu, H., and Zhang, F. (2017). Zircon U-Pb ages and geochemical characteristics study of syenite from Weishan REE deposit, Western Shandong. *Acta Sci. Nat. Univ. Pekin.* 53 (4), 652–666. (in Chinese with English abstract). doi:10.13209/j.0479-8023.2017.010
- Litvinovsky, B. A., Jahn, B. M., Zanzvilevich, A. N., and Shadaev, M. G. (2002). Crystal fractionation in the petrogenesis of an alkali monzodiorite-syenite series: The oshurkovo plutonic sheeted complex, transbaikalia, Russia. *Lithos* 64, 97–130. doi:10.1016/S0024-4937(02)00179-2
- Liu, D. Y., Nutman, A. P., Compston, W., Wu, J. S., and Shen, Q. H. (1992). Remnants of ≥3800 Ma crust in the Chinese part of the Sino-Korean craton. *Geol.* 20, 339–342. doi:10.1130/0091-7613(1992)020<0339:romcit>2.3.co;2
- Liu, Y., Chakhmouradian, A. R., Hou, Z. Q., Song, W. L., and Kynicky, J. (2019). Development of REE mineralization in the giant Maoniyang deposit (Sichuan, China): Insights from mineralogy, fluid inclusions, and trace-element geochemistry. *Min. Depos.* 54, 701–718. doi:10.1007/s00126-018-0836-y
- Liu, Y., Chen, Z. Y., Yang, Z. S., Sun, X., Zhu, Z. M., Zhang, Q. C., et al. (2015). Geochemical and mineralogical characteristics of weathered ore in the dalucao REE deposit, mianning-dechang REE belt, Western sichuan province, southwestern China. *Ore Geol. Rev.* 70, 437–456. doi:10.1016/j.oregeorev.2015.06.009
- Liu, Y. S., Hu, Z. C., Gao, S., Günther, D., Xu, J., Gao, C. G., et al. (2008). *In situ* analysis of major and trace elements of anhydrous minerals by LA-ICP-MS without applying an internal standard. *Chem. Geol.* 257 (1–2), 34–43. doi:10.1016/j.chemgeo.2008.08.004
- Ludwig, K. R. (2003). *Isoplot 3.00: A geochronological toolkit for microsoft excel*. Berkeley Geochronology Center Special Publication. No. 4.
- Macdonald, R., and Scaillet, B. (2006). The central Kenya peralkaline province: Insights into the evolution of peralkaline salic magmas. *Lithos* 91, 59–73. doi:10.1016/j.lithos.2006.03.009
- Maniari, P. D., and Piccoli, P. M. (1989). Tectonic discrimination of granitoids. *Geol. Soc. Am. Bull.* 101 (5), 635–643. doi:10.1130/0016-7606(1989)101<0635:tdog>2.3.co;2
- Martin, R. F. (2006). A-type granites of crustal origin ultimately result from open-system fenitization-type reactions in an extensional environment. *Lithos* 91, 125–136. doi:10.1016/j.lithos.2006.03.012
- Middlemost, E. A. K. (1994). Naming materials in the magma/igneous rock system. *Earth. Sci. Rev.* 37 (3–4), 215–224. doi:10.1016/0012-8252(94)90029-9
- Miyazaki, T., Kagami, H., Shuto, K., Mohan, V. R., and Rajasekaran, K. C. (2000). Rb-Sr geochronology, Nd-Sr isotopes and whole rock geochemistry of Yelagiri and

- Sevattur syenites, Tamil Nadu, South India. *Gondwana Res.* 3, 39–53. doi:10.1016/S1342-937X(05)70056-3
- Pearce, J. A. (1996). Sources and settings of granitic rocks. *Episodes* 19 (4), 120–125. doi:10.18814/epiuiugs/1996/v19i4/005
- Peccerillo, A., and Taylor, S. R. (1976). Geochemistry of Eocene calc-alkaline volcanic rocks from the Kastamonu area, northern Turkey. *Contr. Mineral. Petrol.* 58 (1), 63–81. doi:10.1007/BF00384745
- Pin, C., Gannoun, A., and Dupont, A. (2014). Rapid, simultaneous separation of Sr, Pb, and Nd by extraction chromatography prior to isotope ratios determination by TIMS and MC-ICP-MS. *J. Anal. At. Spectrom.* 29, 1858–1870. doi:10.1039/c4ja00169a
- Qiu, J. X. (1993). *The alkaline rocks in Qin-Bashan area*. Beijing: Geological Publishing House, 1–137. (in Chinese).
- Saccani, E. (2015). A new method of discriminating different types of post-Archean ophiolitic basalts and their tectonic significance using Th-Nb and Ce-Dy-Yb systematics. *Geosci. Front.* 6, 481–501. doi:10.1016/j.gsf.2014.03.006
- Santosh, M. (2010). Assembling north China craton within the columbia supercontinent: The role of double-sided subduction. *Precambrian Res.* 178, 149–167. doi:10.1016/j.precamres.2010.02.003
- Santosh, M., Teng, X. M., He, X. F., Tang, L., and Yang, Q. Y. (2016). Discovery of Neoproterozoic suprasubduction zone ophiolite suite from Yishui Complex in the North China Craton. *Gondwana Res.* 38, 1–27. doi:10.1016/j.gr.2015.10.017
- Smith, M. P., Moore, K., Kavacs'anszki, D., Finch, A. A., Kynicky, J., and Wall, F. (2016). From mantle to critical zone: A review of large and giant sized deposits of the rare Earth elements. *Geosci. Front.* 7 (3), 315–334. doi:10.1016/j.gsf.2015.12.006
- Söderlund, U., Patchett, P. J., Vervoort, J. D., and Isachsen, C. E. (2004). The ¹⁷⁶Lu decay constant determined by Lu-Hf and U-Pb isotope systematics of Precambrian mafic intrusions. *Earth Planet. Sci. Lett.* 219 (3–4), 311–324. doi:10.1016/S0012-821X(04)00012-3
- Sun, S. S., and McDonough, W. F. (1989). “Chemical and Isotopic Systematics of Oceanic Basalts: Implications for Mantle Composition and Processes”. Editors A. D. Saunders and M. J. Norry (London: Geological Society, London, Special Publications 42, 313–345. doi:10.1144/gsl.sp.1989.042.01.19
- Tan, J., Wei, J. H., Tan, W. J., and Guo, D. Z. (2006). Statistic study of diagenesis-mineralization time gap for comagmatic gold deposits. *Geol. Rev.* 52 (01), 54–62. (in Chinese with English abstract). doi:10.16509/j.georeview.2006.01.010
- Tchameni, R., Mezger, K., Nsifa, N. E., and Poulet, A. (2001). Crustal origin of early proterozoic syenites in the Congo craton (ntem complex), south Cameroon. *Lithos* 57, 23–42. doi:10.1016/S0024-4937(00)00072-4
- Tian, J. X., Zhang, R. T., Fan, Y. C., Li, X. Z., Xu, H. Y., and Wang, B. Y. (2002). Geological characteristics and relation with rare Earth elements of alkalic complex in Chishan of Shandong Province. *Shandong Geol.* 18 (1), 21–25. (in Chinese with English abstract).
- Tu, G. Z., Zhang, Y. Q., and Zhao, Z. H. (1984). “The preliminary study on two alkali rich intrusive rocks zones,” in *Granite geology and mineralization: International symposium on granites*. Editors K. Q. Xu and G. C. Tu (Nanjing: Science and Technology Publishing House of Jiangsu), 21–37. (in Chinese).
- Walter, M. J., Bulanova, G. P., Armstrong, L. S., Keshav, S., Blundy, J. D., Gudfinnsson, G., et al. (2008). Primary carbonatite melt from deeply subducted oceanic crust. *Nature* 454, 622–625. doi:10.1038/nature07132
- Wang, C. M., Bagas, L., Deng, J., and Dong, M. M. (2018). Crustal architecture and its controls on mineralisation in the North China Craton. *Ore Geol. Rev.* 98, 109–125. doi:10.1016/j.oregeorev.2018.05.016
- Wei, P. F., Yu, X. F., Li, D. P., Liu, Q., Yu, L. D., Li, Z. S., et al. (2019). Geochemistry, zircon U-Pb geochronology, and Lu-Hf isotopes of the chishan alkaline complex, western shandong, China. *Minerals* 9 (5), 293. doi:10.3390/min9050293
- Wilde, S. A., Zhou, X. H., Nemchin, A. A., and Sun, M. (2003). Mesozoic crust-mantle interaction beneath the north China craton: A consequence of the dispersal of gondwanaland and accretion of asia. *Geol.* 31, 817–820. doi:10.1130/G19489.1
- Wu, F. Y., Li, X. H., Zheng, Y. F., and Gao, S. (2007). Lu-Hf isotopic systematics and their applications in petrology. *Acta Petrol. Sin.* 23 (2), 185–220. (in Chinese with English abstract).
- Wu, F. Y., Lin, J. Q., Wilde, S. A., Zhang, X. O., and Yang, J. H. (2005). Nature and significance of the Early Cretaceous giant igneous event in eastern China. *Earth Planet. Sci. Lett.* 233, 103–119. doi:10.1016/j.epsl.2005.02.019
- Wu, F. Y., Xu, Y. G., Gao, S., and Zheng, J. P. (2008). Lithosphere thinning and destruction of the north China craton. *Acta Petrol. Sin.* 24, 1145–1174. (in Chinese with English abstract).
- Wu, K., Ling, M. X., Sun, W. D., Guo, J., and Zhang, C. C. (2017). Major transition of continental basalts in the early cretaceous: Implications for the destruction of the north China craton. *Chem. Geol.* 470, 93–106. doi:10.1016/j.chemgeo.2017.08.025
- Xie, Y. L., Hou, Z. Q., Yin, S. P., Dominy, S. C., Xu, J. H., Tian, S. H., et al. (2009). Continuous carbonatitic melt-fluid evolution of a REE mineralization system: Evidence from inclusions in the Maoniuping REE Deposit, Western Sichuan, China. *Ore Geol. Rev.* 36 (1–3), 90–105. doi:10.1016/j.oregeorev.2008.10.006
- Xie, Y. L., Xia, J. M., Cui, K., Qu, Y. W., Liang, P., and Zhong, R. C. (2020). Rare Earth elements deposits in China: Spatio-temporal distribution and ore-forming processes. *Chin. Sci. Bull.* 65, 3794–3808. (in Chinese with English abstract). doi:10.1360/TB-2020-0371
- Xu, W. G., Fan, H. R., Hu, F. F., Santosh, M., Yang, K. F., Lan, T. G., et al. (2015). Geochronology of the guilaizhuang gold deposit, Luxi block, eastern North China craton: Constraints from zircon U-Pb and fluorite-calcite Sm-Nd dating. *Ore Geol. Rev.* 65, 390–399. doi:10.1016/j.oregeorev.2014.10.010
- Xu, Y. G., Huang, X. L., Ma, J. L., Wang, Y. B., Iizuka, Y., Xu, J. F., et al. (2004). Crust-mantle interaction during the tectono-thermal reactivation of the north China craton: Constraints from SHRIMP zircon U-Pb chronology and geochemistry of mesozoic plutons from Western shandong. *Contrib. Mineral. Petrol.* 147, 750–767. doi:10.1007/s00410-004-0594-y
- Xu, Z., Zhao, Z. F., and Zheng, Y. F. (2012). Slab-mantle interaction for thinning of cratonic lithospheric mantle in North China: Geochemical evidence from Cenozoic continental basalts in central Shandong. *Lithos* 146–147, 202–217. doi:10.1016/j.lithos.2012.05.019
- Yan, G. H., Cai, J. H., Ren, K. X., Mu, B. L., Li, F. T., and Chu, Z. Y. (2008). Nd, Sr and Pb isotopic geochemistry of late-mesozoic alkaline-rich intrusions from the tanlu fault zone: Evidence of the magma source. *Acta Petrol. Sin.* 24 (6), 1223–1236. (in Chinese with English abstract).
- Yang, C. X., and Santosh, M. (2020). Ancient deep roots for mesozoic world-class gold deposits in the north China craton: An integrated genetic perspective. *Geosci. Front.* 11, 203–214. doi:10.1016/j.gsf.2019.03.002
- Yang, D. B., Xu, W. L., Pei, F. P., Yang, C. H., and Wang, Q. H. (2012a). Spatial extent of the influence of the deeply subducted South China Block on the southeastern North China Block: Constraints from Sr-Nd-Pb isotopes in Mesozoic mafic igneous rocks. *Lithos* 136–139, 246–260. doi:10.1016/j.lithos.2011.06.004
- Yang, F., Santosh, M., Glorie, S., Jepson, G., Xue, F., and Kim, S. W. (2020). Mesozoic multiple exhumation in the shandong peninsula, eastern North China craton: Implications for lithospheric destruction. *Lithos* 370, 105597. doi:10.1016/j.lithos.2020.105597
- Yang, F., Santosh, M., and Kim, S. W. (2018b). Mesozoic magmatism in the eastern North China craton: Insights on tectonic cycles associated with progressive craton destruction. *Gondwana Res.* 60, 153–178. doi:10.1016/j.gr.2018.04.003
- Yang, F., Santosh, M., and Tang, L. (2018a). Extensive crustal melting during craton destruction: Evidence from the mesozoic magmatic suite of junan, eastern North China craton. *J. Asian Earth Sci.* 157, 119–140. doi:10.1016/j.jseas.2017.07.010
- Yang, J. H., Wu, F. Y., Chung, S. L., Wilde, S. A., and Chu, M. F. (2006). A hybrid origin for the qianshan A-type granite, northeast China: Geochemical and Sr-Nd-Hf isotopic evidence. *Lithos* 89 (1–2), 89–106. doi:10.1016/j.lithos.2005.10.002
- Yang, J. H., Wu, F. Y., Xie, L. W., and Liu, X. M. (2007). Petrogenesis and tectonic implications of kuangdonggou syenites in the liaodong peninsula, east north China craton: Constraints from *in-situ* zircon U-Pb ages and Hf isotopes. *Acta Petrol. Sin.* 23 (2), 263–276. (in Chinese).
- Yang, J. H., Xu, L., Sun, J. F., Zeng, Q., Zhao, Y. N., Wang, H., et al. (2021). Geodynamics of decratonization and related magmatism and mineralization in the North China Craton. *Sci. China Earth Sci.* 64 (9), 1409–1427. doi:10.1007/s11430-020-9732-6
- Yang, K. F., Fan, H. R., Santosh, M., Hu, F. F., and Wang, K. Y. (2011). Mesoproterozoic carbonatitic magmatism in the Bayan Obo deposit, Inner Mongolia, North China: Constraints for the mechanism of super accumulation of rare Earth elements. *Ore Geol. Rev.* 40 (1), 122–131. doi:10.1016/j.oregeorev.2011.05.008
- Yang, K. F., Fan, H. R., Santosh, M., Hu, F. F., Wilde, S. A., Lan, T. G., et al. (2012b). Reactivation of the archaic lowercrust: Implications for zircon geochronology, elemental and Sr-Nd-Hf isotopic geochemistry of late mesozoic granitoids from northwestern jiaodong terrane, the north China craton. *Lithos* 146, 112–127. doi:10.1016/j.lithos.2012.04.035
- Yang, X. Y., Sun, W. D., Zhang, Y. X., and Zheng, Y. F. (2009). Geochemical constraints on the Genesis of the bayan Obo Fe-Nb-REE deposit in inner Mongolia, China. *Geochim. Cosmochim. Acta* 73 (5), 1417–1435. doi:10.1016/j.gca.2008.12.003
- Yang, Y. H., Zhang, H. F., Chu, Z. Y., Xie, L. W., and Wu, F. Y. (2010). Combined chemical separation of Lu, Hf, Rb, Sr, Sm and Nd from a single rock digest and precise and accurate isotope determinations of Lu-Hf, Rb-Sr and Sm-Nd isotope systems using Multi-Collector ICP-MS and TIMS. *Int. J. Mass Spectrom.* 290, 120–126. doi:10.1016/j.ijms.2009.12.011

- Yu, X. F., Tang, H. S., and Li, D. P. (2014). Study on the mineralization of Chishan rare Earth element deposit related to alkaline rock, Shandong Province. *Acta Geol. Sin. - Engl. Ed.* 88 (2), 480–481. doi:10.1111/1755-6724.12373_31
- Yu, X. F., Tang, H. S., Han, Z. Z., and Li, C. Y. (2010). Geological characteristics and origin of rare Earth elements deposits related with alkaline rock in the Chishan-Longbaoshan area, Shandong Province. *Acta Petrol. Sin.* 84 (3), 407–417. (in Chinese with English abstract).
- Yuan, H. L., Gao, S., Liu, X. M., Li, H. M., Gunther, D., and Wu, F. Y. (2004). Accurate U-Pb age and trace element determinations of zircon by laser ablation-inductively coupled plasma-mass spectrometry. *Geostand. Geoanal. Res.* 28 (3), 353–370. doi:10.1111/j.1751-908X.2004.tb00755.x
- Zeng, J. P., Lin, W., Qiu, H. B., Wei, W., Meng, L. T., Chu, Y., et al. (2022). When did the large-scale extensional tectonics begin in North China Craton? *Tectonophysics* 840, 229563. doi:10.1016/j.tecto.2022.229563
- Zhai, M. G., and Santosh, M. (2011). The early precambrian odyssey of the north China craton: A synoptic overview. *Gondwana Res.* 20, 6–25. doi:10.1016/j.gr.2011.02.005
- Zhai, M. G., Yang, J. H., Fan, H. R., Miao, L. C., and Li, Y. G. (2002). A large-scale cluster of gold deposits and metallogenesis in the eastern North China Craton. *Int. Geol. Rev.* 44 (5), 458–476. doi:10.2747/0020-6814.44.5.458
- Zhang, B., Liu, S. F., Lin, C. F., Shen, W. J., and Li, X. Y. (2020). Reconstruction of the stress regime in the Jiaolai Basin, East Asian margin, as decoded from fault-slip analysis. *J. Struct. Geol.* 141 (2020), 104190–190. doi:10.1016/j.jsg.2020.104190
- Zhang, H. F., Sun, M., Zhou, M. F., Fan, W. M., Zhou, X. H., and Zhai, M. G. (2004). Highly heterogeneous late mesozoic lithospheric mantle beneath the north China craton: Evidence from Sr-Nd-Pb isotopic systematics of mafic igneous rocks. *Geol. Mag.* 141 (1), 55–62. doi:10.1017/S0016756803008331
- Zhang, H. F., Sun, M., Zhou, X. H., Fan, W. M., Zhai, M. G., and Yin, J. F. (2002). Mesozoic lithosphere destruction beneath the north China craton: Evidence from major-trace-element and Sr-Nd-Pb isotope studies of Fangcheng basalts. *Contrib. Mineral. Petrol.* 144, 241–254. doi:10.1007/s00410-002-0395-0
- Zhang, H. F., Sun, M., Zhou, X. H., and Ying, J. F. (2005). Geochemical constraints on the origin of mesozoic alkaline intrusive complexes from the north China craton and tectonic implications. *Lithos* 81 (1–4), 297–317. doi:10.1016/j.lithos.2004.12.015
- Zhang, H. F., Ying, J. F., Shimoda, G., Kita, N. T., Morishita, Y., Shao, J. A., et al. (2007a). Importance of melt circulation and crust-mantle interaction in the lithospheric evolution beneath the north China craton: Evidence from mesozoic basalt-borne clinopyroxene xenocrysts and pyroxenite xenoliths. *Lithos* 96, 67–89. doi:10.1016/j.lithos.2006.10.002
- Zhang, H. F., Zhu, R. X., Santosh, M., Ying, J. F., Su, B. X., and Hu, Y. (2013). Episodic widespread magma underplating beneath the north China craton in the phanerozoic: Implications for craton destruction. *Gondwana Res.* 23, 95–107. doi:10.1016/j.gr.2011.12.006
- Zhang, S. H., Zhao, Y., Davis, G. A., Ye, H., and Wu, F. (2014). Temporal and spatial variations of mesozoic magmatism and deformation in the north China craton: Implications for lithospheric thinning and decratonization. *Earth. Sci. Rev.* 131, 49–87. doi:10.1016/j.earscirev.2013.12.004
- Zhang, X. M., Zhang, Y. Q., and Ji, W. (2007b). Fault distribution patterns of the Luxi Block, Shandong, and Mesozoic sedimentary-magmatic-structural evolution sequence. *J. Geomechanics* 13, 163–172. (in Chinese with English abstract).
- Zhao, G. C., Sun, M., Wilde, S. A., and Li, S. Z. (2005). Late archean to paleoproterozoic evolution of the north China craton: Key issues revisited. *Precambrian Res.* 136, 177–202. doi:10.1016/j.precamres.2004.10.002
- Zhao, G. C., Wilde, S. A., Cawood, P. A., and Sun, M. (2001). Archean blocks and their boundaries in the north China craton: Lithological, geochemical, structural and P-T path constraints and tectonic evolution. *Precambrian Res.* 107, 45–73. doi:10.1016/S0301-9268(00)00154-6
- Zhao, G., and Zhai, M. (2013). Lithotectonic elements of precambrian basement in the north China craton: Review and tectonic implications. *Gondwana Res.* 23, 1207–1240. doi:10.1016/j.gr.2012.08.016
- Zhao, J. X., Shiraiishi, K., Ellis, D. J., and Sheraton, J. W. (1995). Geochemical and isotopic studies of syenites from the Yamato Mountains, East Antarctica: Implications for the origin of syenitic magmas. *Geochim. Cosmochim. Acta* 59, 1363–1382. doi:10.1016/0016-7037(95)00050-A
- Zhao, Z. F., Liu, Z. B., and Chen, Q. (2017). Melting of subducted continental crust: Geochemical evidence from Mesozoic granitoids in the Dabie-Sulu orogenic belt, east-central China. *J. Asian Earth Sci.* 145, 260–277. doi:10.1016/j.jseas.2017.03.038
- Zheng, J. P. (2009). Comparison of mantle-derived materials from different spatiotemporal settings: Implications for destructive and accretional processes of the north China craton. *Sci. Bull. (Beijing)*. 54, 3397–3416. doi:10.1007/s11434-009-0308-y
- Zheng, Y. F., Xu, Z., Zhao, Z. F., and Dai, L. Q. (2018). Mesozoic mafic magmatism in North China: Implications for thinning and destruction of cratonic lithosphere. *Sci. China Earth Sci.* 61, 353–385. doi:10.1007/s11430-017-9160-3
- Zhu, R. X., Chen, L., Wu, F. Y., and Liu, J. L. (2011). Timing, scale and mechanism of the destruction of the North China Craton. *Sci. China Earth Sci.* 54, 789–797. doi:10.1007/s11430-011-4203-4
- Zhu, R. X., and Xu, Y. G. (2019). The subduction of the west Pacific plate and the destruction of the North China Craton. *Sci. China Earth Sci.* 62, 1340–1350. doi:10.1007/s11430-018-9356-y
- Zhu, R. X., Yang, J. H., and Wu, F. Y. (2012). Timing of destruction of the north China craton. *Lithos* 149, 51–60. doi:10.1016/j.lithos.2012.05.013